This is the peer reviewed version of the following article:

J. Dobrić, A. Filipović, N. Baddoo, Z. Marković, D. Buđevac, Design procedures for cold-formed stainless steel equal-leg angle columns, Thin-Walled Structures., (2020).

https://doi.org/10.1016/j.tws.2020.107210

Design procedures for cold-formed stainless steel equal-leg angle columns

Jelena Dobrić [a,*], Aljoša Filipović[a], Nancy Baddoo[b], Zlatko Marković[a], Dragan Buđevac[a]

[a] University of Belgrade, Faculty of Civil Engineering, Serbia

[b] Steel Construction Institute, United Kingdom

Corresponding author: Jelena Dobrić, jelena@imk.grf.bg.ac.rs (phone: +381-11-3218-626)

Highlights:

1. FE parametric studies including geometric and material nonlinearity performed.
2. Accuracy of European and Australian codified procedures assessed.
3. Proposal provided for different buckling curves per stainless steel family.
4. Reliability analysis of existing and proposed design recommendations carried out.

Design procedures for cold-formed stainless steel equal-leg angle columns

Abstract

Currently, there is still no explicit design approach for cold-formed stainless steel columns with equal-leg angle sections in Europe. A comprehensive numerical investigation, validated by the available experiments collected in the literature, has therefore been undertaken to provide benchmark data for the assessment of design procedures for cold-formed stainless steel angle columns currently adopted in European and Australian codes. Minor-axis flexural buckling, as well as flexural-torsional buckling have been considered. In total, 27 different cross-section sizes covering both slender and non-slender sections, and a wide range of column slenderness values have been examined including austenitic, duplex and ferritic grades. On the basis of the experimental and numerical results, new design recommendations for cold-formed stainless steel equal-leg angle columns have been made per family of stainless steel. The suitability of the proposals was confirmed by means of a reliability analysis.

Key-words: Stainless steel; Angle section; Cold-forming; Flexural-torsional buckling; Flexural buckling; Finite Element Modelling; Design.

1. Introduction

Along with the development of more resistant and sustainable engineering structures, there is growing interest in the use of high-efficiency construction materials such as stainless steel. Stainless steel has many desirable characteristics that can be utilized in a wide variety of construction applications. Due to high chromium content, this material has the ability to form a self-repairing protective oxide layer that provides excellent corrosion resistance. In addition, nickel, which is present in the chemical composition of austenitic and duplex alloys, improves their formability, weldability and toughness. The high strength, higher levels of crevice and stress corrosion cracking resistance of duplex stainless steels—presenting a mixed microstructure of austenite and ferrite—provide a number of economic benefits in weight-sensitive structures like bridges or offshore topsides in marine and other aggressive environments [1], [2].

In recognition of the many beneficial properties of stainless steel, numerous research projects have been carried out over the last few decades to generate structural design rules that guide the development of international design codes. Although significant experimental work on beam and column strength of cold-formed stainless steel hollow sections has been carried out, research on stainless steel open cross-section members has been less studied. Most research on non-doubly symmetric stainless steel columns has been concerned with local, distortional, flexural-torsional and flexural buckling behaviour with respect to lipped channel sections [1], plain channels sections [4], [5] and equal-leg angle sections [6], [7], [8], [9].

The work explained herein expands the research scope to structural cold-formed stainless steel equal-leg angle columns under axial compressive actions, including Finite Element (FE) analysis to assess the impact of geometrical and material non-linearity and provide a more general evaluation of their behaviour. The current specification approaches involving both flexural-torsional buckling and flexural buckling are evaluated by a reliability-based method and the potential for their improvement and appropriateness for cold-formed stainless steel angle columns are discussed.

The structural response of an angle column is strongly affected by its geometry. Despite basic simplicity and adaptability of the angle shape, the location of the shear centre at the intersection of angle legs and its non-coincidence with the section's centroid lead to a negligible warping resistance and low torsional stiffness (additionally considering the small beneficial effect of rounded corners in the cases of cold-formed angles).

As a consequence, cold-formed steel equal angle columns exhibit two major buckling modes or their combination: flexural-torsional buckling (FTB) about the major cross-section principal axis in the intermediate and low slenderness domain and flexural buckling (FB) about the minor cross-section principal axis in the high and intermediate slenderness domain. Besides, due to the low torsional rigidity, short equal-leg angle columns could be susceptible to the torsional buckling (TB) mode whose failure shape corresponds to the local buckling (LB) shape [10].

The difficulty in assessing stability of equal-leg angle columns (the prevalence of FTB or FB) is especially noticeable in the case of slender sections. The deformation and stress redistribution upon the elastic LB of angle legs reduce effective section properties and cause the effective centroid to shift along the axis of symmetry towards the corner, which, in turn, results in an interaction between the initial axial load and additional bending. Furthermore, the inevitable presence of initial imperfections and end eccentricity of loading acting in combination with the effective centroid shift additionally affects the occurrence of buckling and subsequent failure. As the cross-section is asymmetric, distribution of axial stresses in the cross-section strongly depends on the direction of total eccentricity along the axis of symmetry—towards the tips of the legs or to the corner (one causing compressive yielding of the leg tips, the other causing compressive yielding of the section corner). The mentioned effects have a more important role in pin-ended columns than in fixed-ended columns, because of the ability of fixed-ended boundary conditions to prevent additional bending caused by the shift of the effective centroid, otherwise induced in pin-ended columns. It should be noted also that an increase of the leg widths increases the distance between the shear centre and the section centroid (point of application of the axial load). This increases the tendency of the angle to rotate and potentially leads to FTB failure in the entire overall slenderness range.

The significantly different post buckling behaviours of the fixed- and pin-ended short-to-intermediate equal-leg angle columns provides the explanation for the noticeable discrepancy between their ultimate capacities [11]. The differences concerning the buckling and post-buckling behaviour of the aforementioned angle columns are highlighted in comprehensive investigation [11], [12], [13] in which a new approaches for their design based on the Direct Strength Method (DSM) have been developed. Out of the results reported in these publications, the following deserve to be mentioned: (i) both the fixed- and pin-ended columns featured by

similar buckling performances: critical load decreases gradually with column length and the critical buckling mode always exhibits a single half-wave. The critical buckling modes of columns with short-to-intermediate lengths exhibit interaction of torsion and major-axis flexure—there is an increasing amount of major-axis flexure with increasing column's length. (ii) Both the fixed- and pin-ended columns display post-buckling behaviours featured by the simultaneous effects of cross-section torsional rotations and corner displacements (translations) that are result of major- and minor-axis bending. The minor-axis flexural displacements significantly affect the column post-buckling response: the postcritical strength reserve and distributions of longitudinal normal stresses. This impact is more pronounced in the pin-ended columns than in the fixed-ended columns. (iii) The participation of minor-axis flexure on the critical flexural-torsional buckling modes appears in the post-buckling stage as a result of the longitudinal variation of the torsional rotations, causing nonlinear cross-section longitudinal stress distributions that are associated with effective centroid shifts. (iv) Both the column post-buckling behaviour and effective centroid shift effects (the latter exhibit in pin-ended columns) are length-dependent; this length-dependence is associated with the column critical buckling mode features [11], [12], [13].

Our paper fills the gap created by the lack of experimental results and explicit design guidelines for CFSS equal-leg angle columns. A comprehensive numerical investigation is presented with the aim of investigating the structural behaviour of pin-ended angle columns and assessing the suitability of the current European and Australian/New Zealand specification approaches for FB and FTB resistance predictions. This paper begins with a literature review and detailed interpretation of the design procedures stated in the mentioned specifications. The qualitative FE modelling is then described. The developed models are calibrated and validated against experiments performed by Dobrić et al. [8]. A quantitative parametric study is subsequently performed to generate reliable data over a wider range of column non-dimensional slenderness values, including three most significant stainless steel families − austenitic, duplex and ferritic. The codified procedures are then evaluated through comparisons between experimental/numerical data and equivalent design data and the assessment of the safety factor γ_{M1} and resistance factor ϕ_c.

2. Literature review

The theoretical and experimental observations on cold-formed carbon steel (CFS) angle columns are the basis for a better understanding of the structural behaviour of cold-formed stainless steel (CFSS) angle columns. Despite basic similarities between CFSS and CFS angle columns that relate to cross-sectional geometry and impact of initial imperfections, the pronounced material nonlinear behaviour of stainless steel should be accounted for in design. The buckling response and design of CFS angle columns have been, and continue to be, the subject of extensive scientific investigations across the globe, of which, the most relevant references are mentioned below.

Based on an evaluation of the available test data, Peköz [14] noticed the significant influence of initial sweep (out-of-straightness) of an angle column on its compression resistance. It was found that the sweep in the plane of symmetry toward the section corner has a significantly greater influence than the sweep in other directions. Based on this outcome, the author suggested to account for an additional moment of $P{\cdot}L/1000$ (where P is the compressive axial load and L is the column height) about the minor-principal axis in the design of axially compressed angle members. This recommendation was introduced in the 1986 edition of the AISI Specification. Popovic et al. [15] performed a series of experiments on fixed-ended and pin-ended CFS angle columns, covering both non-slender and slender sections, to study their FB and FTB response. The authors noticed that the compressive capacity of columns with slender angle sections is strongly affected by the eccentricity direction at the columns' ends. The higher level of compressive stresses at the corners of the section, caused by load eccentricity applied towards the corner, reduces the stress level at the legs' tips and leads to greater column strength in comparison with corresponding columns with oppositely applied eccentricity (toward the leg tips). It was recommended that the required additional moment about the minor-principal axis due to initial sweep—stated in the established Australian and American cold-formed specifications—should only be applied to those angle columns with slender sections (subjected to elastic local buckling bellow yield strength). As a consequence of this finding, a correction was made in the next edition of the AISI and AS/NZS specification. Popovic et al. [16] continued their study performing experiments on 11 pin-ended CFS columns with slender equal-leg angle sections under three different eccentricity conditions. Based on the obtained results, the authors proposed that the procedure for the FTB

failure mode should be omitted from the codified method stated in AISI and AS/NZS specifications and only minor-axis FB should be considered.

Young [17] conducted experimental tests on fixed-end CFS plain angle columns under axial compression. The angle sections were press-braked from high strength structural steel sheets. The author proposed new design equations to predict the buckling resistance of axially compressed fixed-ended CFS columns, including both slender and non-slender angle sections. The new procedure covers only FB and ignores elastic TB and FTB stress in design calculations. It is also recommended that the additional moment of $P{\cdot}L/1000$ can also be ignored in calculating the column design strengths for both slender and non-slender CFS plain angle sections. Ellobody and Young [18] reported a comprehensive numerical parametric study on CFS angles compressed between fixed ends over different column lengths to assess existing design recommendations. The numerical results emphasized the conservatism of the established codified procedures and showed good agreement with the predictions obtained by the new design equations proposed in Young's previous investigation [17]. Rasmussen [10] developed a new design method for pin-ended CFS columns with slender equal angle sections considering the shift of the effective centroid and loading eccentricity. The design procedure, based on the beam–column approach, excludes the torsional stresses in determining the compression and bending member resistance and considers the shift of the effective centroid taking into account the actual post-buckling stress distribution. The reason for ignoring overall TB is that it is already accounted for in the LB reduction in determining the effective cross-section area. In parallel, the author proposed a simple design model for axially compressed angles introducing a reduction factor to account for the effect of an additional bending moment caused by the shift in the effective neutral axis. Chodraui et al. [19] performed an accuracy assessment of the predicted buckling resistances of axially loaded CFS equal angle columns determined by codified procedures based on the effective width method (EWM) and DSM using experiments, numerical methods and imperfection sensitivity studies. Contrary to previous findings, the authors' results indicated that the design approach which ignores TB as an overall mode may lead to unconservative predictions. It was concluded that the established codified procedures should treat LB and TB as both a local-plate mode and an overall-torsional mode. Dinis and Camotim [12] developed a new design approach for thin-walled fixed-ended and pin-ended angle columns, based on DSM, which includes the use

of length-dependent flexural–torsional strength curves and considers the interaction between two overall modes, FTB and FB. Landesmann et al. [13] performed an experimental investigation of CFS pin-ended equal angle columns. The geometry of specimens was chosen to provide the transition from the FTB to FB mode. Based on experiments and a subsequent numerical parametric study, an assessment of the proposed DSM-based design approach [12] was carried out, which was shown to offer a high level of accuracy in the prediction of strengths of CFS equal angle columns.

Although extensive efforts have been devoted to determining the compressive capacity of CFS angle columns, the design of compressed CFSS angle columns, including both experimental and numerical research, has attracted less attention. Among other types of cross-sections, Kuwamura [6] performed experiments on 12 cold-formed stainless steel stub column specimens comprising plain equal-leg angles made of austenitic EN1.4301 and EN1.4318 grades. Zhang et al. [7] experimentally and numerically investigated FTB of fixed-ended cold-formed austenitic stainless steel equal-leg angle columns. The obtained results were used to evaluate current European and Australian specifications and, in parallel, the DSM-based design approach [12], for FTB predictions. Comparative analysis indicates that the EWM employed in codified design procedures leads to a high level of conservatism and data scatter, whereas the DSM-based design method, initially developed for CFS angles, significantly improves design accuracy, although with unsafe strength predictions for a significant number of data. Dobrić et al. [8] performed 11 column tests including short, intermediate length and long equal-leg angle specimens produced from lean duplex grade EN1.4162.

3. Existing design methods

In this section, the European [20] and Australian/New Zealand [21] specifications for the design of stainless steel thin-walled members are summarised and the bases for assessing the structural responses of CFSS plain equal-leg angle columns are outlined.

The mentioned specifications permit the use of an EWM in the design of compressed thin-walled members, which treats cross-sections as a collection of plain plate elements and investigates LB of each element separately. The calculation method used to determine the effective width of the plate elements introduces a

reduction factor, which depends on the plate support conditions, loading conditions, yield strength of the material and plate width-to-thickness ratio.

According to Clause 5.2.2, EN 1993-1-4 [20], if the slenderness width-to-thickness ratio $\bar{b}/t$ (for a cold-formed angle, $\bar{b}$ is the notional flat leg width, measured from the midpoint of the corner up to the free end, and t is the leg thickness) of the equal-leg angle is larger than $14 \cdot \varepsilon$ (ε is the material parameter), the angle section is classified as Class 4. Clause 5.2.3 [20] provides the procedure for determining effective widths in Class 4 cross-sections: the procedure is based on the method for carbon steel provided in EN 1993-1-5 [22] but prescribes more conservative expressions for reduction factors to allow for stainless steel material non-linearity. For outstand elements, the reduction factor should be taken as follows:

$$\rho = \frac{1}{\bar{\lambda}_{\mathrm{p}}} - \frac{0.188}{\bar{\lambda}_{\mathrm{p}}^{\,2}} \leq 1 \qquad \text{for outstand elements with } \bar{\lambda}_{\mathrm{p}} \geq 0.748 \tag{1}$$

where:

$$\bar{\lambda}_{\mathrm{p}} = \frac{\bar{b}/t}{28.4\varepsilon\sqrt{k_{\sigma}}} \tag{2}$$

In Eq. (2), k_{σ} is the plate buckling coefficient, taken as 0.43 for outstand elements in uniform compression.

Clause 5.4 [20] provides a procedure to determine the design buckling resistance of compression members. The design approach, based on the Perry-Robertson formulation, employed a linear expression for the imperfection parameter $\eta = \alpha\left(\bar{\lambda} - \bar{\lambda}_0\right)$, where α and $\bar{\lambda}_0$ are constants which capture the effects of geometric imperfections and residual stresses on the column strength. The effect of material nonlinearity is not explicitly accounted for in the member buckling formulations. Moreover, the design rules do not explicitly state the values of neither the imperfection factor α nor the non-dimensional limiting slenderness $\bar{\lambda}_0$ for stainless steel angles in the relevant buckling plane depending both on the manufacturing process and stainless steel grade. Instead, only three sets of buckling curves, each with different values for the constants α and $\bar{\lambda}_0$, are set out: the parameters α and $\bar{\lambda}_0$ are equal 0.49 and 0.40, respectively, for FB of cold-formed open cross-sections, 0.76 and 0.20, respectively, for FB of welded sections, whereas for TB and FTB, they are equal 0.34 and 0.20, respectively. However, the experimental research over the last decade has shown that the EN 1993-1-4 buckling curves may be optimistic for CFSS sections, and that there is a difference in

column buckling responses among the families of stainless steels. Based on these findings, the fourth edition of the Design Manual for Structural Stainless Steel [23] revised the buckling curves for FB and adopted a more conservative curve (α = 0.76 $\bar{\lambda}_0$ = 0.2), irrespective of the stainless steel alloy, for FB for CFSS angle sections.

The buckling resistance of a stainless steel compression member $N_{\mathrm{b,Rd}}$, is obtained from Eq. (3):

$$N_{\mathrm{b,Rd}} = \frac{\chi A f_{\mathrm{y}}}{\gamma_{\mathrm{M1}}} \tag{3}$$

where f_{y} is the material yield strength, taken as the 0.2% proof strength, A is the cross-sectional area, taken as the gross cross-sectional area for Class 1, 2 and 3 sections and an effective cross-sectional area A_{eff} for Class 4 sections, and γ_{M1} is the partial resistance factor for the member. The non-dimensional buckling reduction factor χ is given by Eq. (4)

$$\chi = \frac{1}{\phi + \sqrt{\phi^2 - \bar{\lambda}^2}} \leq 1.0 \tag{4}$$

where $\bar{\lambda}$ is the non-dimensional column slenderness, taken as the square root of the ratio of the yield load ($N_{\mathrm{y}} = A{\cdot}f_{\mathrm{y}}$) to the elastic critical buckling load N_{cr} and ϕ is defined as

$$\phi = 0.5\left(1 + \eta + \bar{\lambda}^2\right) \tag{5}$$

Clause 6.2.3 of EN1993-1-3 [24] provides expressions (6.33a) and (6.35) for determining the elastic critical torsional and FTB loads, respectively.

Single angles loaded through one leg fail by interaction between the axial force and biaxial bending. The design procedure stated in Annex BB of EN 1993-1-1 [25] treats this interaction by adopting a non-dimensional effective (modified) slenderness ratio instead of a geometrical one in the Perry-Robertson formulae under the condition that both ends of the column are welded or connected by at least two bolts. For other end and load conditions, the angle columns should be designed for the actual end eccentricities using appropriate interaction equations. Besides, for columns with non-symmetric slender (Class 4) cross-sections, allowance shall be made for the additional moment due to the eccentricity of the centroid of the effective cross-section with respect to the centroid of the gross cross-section. For stainless steel equal-leg angle

columns with Class 4 cross-sections, Eq. (6), stated in Clause 6.1.9 of EN 1993-1-3 and Eq. (7), provided in Clause 5.5 of EN 1993-1-4, take into account interaction effects between compressive axial load and uniaxial bending moment about the minor-axis FB induced by the shift of the effective centroid.

$$\frac{N_{\mathrm{Ed}}}{A_{\mathrm{eff}} f_{\mathrm{y}}/\gamma_{\mathrm{M0}}} + \frac{N_{\mathrm{Ed}} e_{\mathrm{Nz}}}{W_{\mathrm{eff,z,min}}\, f_{\mathrm{y}} \,/\, \gamma_{\mathrm{M0}}} \leq 1.0 \tag{6}$$

$$\frac{N_{\mathrm{Ed}}}{\left(N_{\mathrm{b,Rd}}\right)_{\mathrm{min}}} + k_{\mathrm{z}} \left(\frac{N_{\mathrm{Ed}} e_{\mathrm{Nz}}}{W_{\mathrm{eff,z}}\, f_{\mathrm{y}} \,/\, \gamma_{\mathrm{M1}}} \right) \leq 1.0 \tag{7}$$

In the above expression, N_{Ed} is the applied design value of the axial compression load; e_{Nz} is the effective centroid shift along the major principal axis when the cross-section is subject to uniform compression; A_{eff} is the effective area of the cross-section when subjected to uniform compression; $W_{\mathrm{eff,z}}$ is the effective section modulus for the *z* axis; $(N_{\mathrm{b,Rd}})_{\mathrm{min}}$ is the smallest value of the design buckling load $N_{\mathrm{b,Rd}}$ for the following four buckling modes: FB about the *y* axis, FB about the *z* axis, TB and TFB. The interaction factor k_{z} can be obtained as follows:

$$k_{\mathrm{z}} = 1.0 + 2\left(\bar{\lambda}_{\mathrm{z}} - 0.5\right) \frac{N_{\mathrm{Ed}}}{\left(N_{\mathrm{b,Rd}}\right)_{\mathrm{min1}}} \qquad \text{but} \qquad 1.2 \leq k_{\mathrm{z}} \leq 1.2 + 2\frac{N_{Ed}}{\left(N_{\mathrm{b,Rd}}\right)_{\mathrm{min1}}} \tag{8}$$

where $(N_{\mathrm{b,Rd}})_{\mathrm{min1}}$ is the smallest value of $N_{\mathrm{b,Rd}}$ for the following three buckling modes: FB about the *z* axis, TB and TFB.

Clauses 2.2 and 2.3 of the Australian specification AS/NZS 4673 [21] (based on the American standard SEI/ASCE-8 [26]) adopt provisions from the AISI Specification for cold-formed carbon steel [27] for determining the effective width factor for uniformly compressed stiffened and unstiffened elements (Winter's plate buckling curves), using following equation:

$$\rho = \frac{1 - \frac{0.22}{\lambda}}{\lambda} \leq 1.0 \tag{9}$$

where λ is the slenderness ratio of the plate element and can be obtained through:

$$\lambda = \left(\frac{1.052}{\sqrt{k}}\right)\left(\frac{b}{t}\right)\left(\sqrt{\frac{f^*}{E_0}}\right) \tag{10}$$

where *b* is the flat width of element excluding radii and *k* is the plate buckling coefficient (taken as 0.5 for uniformly compressed unstiffened elements), f^* is the design stress in the compression element calculated on the basis of the effective design width and E_0 is the initial modulus of elasticity.

According to Clause 3.4.1 [21], the design compressive axial force shall be calculated as a product of ϕ_c and N_c, where ϕ_c is the strength reduction factor for members in compression and N_c is defined as follows:

$$N_c = A_e f_n \tag{11}$$

where A_e is the effective area calculated under buckling stress f_n, which is the least of the FB, TB and FTB stresses.

To allow for the nonlinear stress-strain response and gradual yielding of the stainless steel, the AS/NZS specification proposes an iterative design procedure employing the tangent-modulus approach. For sections not subject to TB or FTB, the FB stress is defined as

$$f_n = \frac{\pi^2 E_t}{(KL/r)^2} \leq f_y \tag{12}$$

where E_t is the tangent modulus in compression corresponding to the buckling stress, K is the effective length factor, L is the unbraced length of the member and r is the radius of gyration of the gross cross-section. The tangent modulus E_t under the buckling stress f, determined from the Ramberg-Osgood relationship, is provided in Appendix B [21]. The tangent-modulus approach necessitates an iterative solution procedure to solve Eq. (12) because the tangent modulus depends on the stress level σ at the point where the inelastic buckling stress f_n should be determined. The predictive expressions for TB and FTB resistance, given in Clauses 3.4.3 and 3.4.4 also introduce the tangent modulus.

As an alternative to the iterative method, an explicit design approach is also proposed. The calculation procedure, based on the Perry-Robertson equation used in EN 1993-1-4, includes a nonlinear expression for the imperfection parameter η:

$$\eta = \alpha\left(\left(\bar{\lambda} - \bar{\lambda}_1\right)^{\beta} - \bar{\lambda}_0\right) \tag{13}$$

In this procedure, the following expression for the FB stress f_n is given:

$$f_n = \frac{f_y}{\phi + [\phi^2 - \bar{\lambda}^2]^{0,5}} \leq f_y \tag{14}$$

where parameter ϕ is defined by expression which is identical to Eq. (5).

This choice of imperfection parameter was based on the investigation carried out by Rasmussen and Rondal [28], [29]. In Eq. (13), the parameters α, β, $\bar{\lambda}_0$ and $\bar{\lambda}_1$ are used to account for the impact of the varying

degrees of nonlinearity displayed by the different stainless steel grades on the predicted compressive column capacity. For austenitic (EN 1.4301), ferritic (EN 1.4003) and duplex (EN 1.4432) grades, the parameters α, β, λ_0 and λ_1 are listed in Table 1.

Table 1. Values of α, β, λ_0 and λ_1 depending on stainless steel grade, in AS/NZS 4673.

Parameters	Stainless steel grades		
	Austenitic	Ferritic	Duplex
α	1.59	0.94	1.16
β	0.28	0.15	0.13
λ_0	0.55	0.56	0.65
λ_1	0.20	0.27	0.42

For sections subject to TB, f_n is defined by Eq. 3.4.3(2), Clause 3.4.3, whereas for FTB, f_n shall be calculated using Eq. 3.4.4(1), Clause 3.4.4. It can be seen that a typing error is probably included in Eq. 3.4.4(1), hence this expression should be adequately corrected by putting the second term $4\beta\sigma_{ey}\sigma_t$ under the square root [4], as stated in Clause 3.4.3, SE/ASCE 8-02 [26]:

$$f_n = \frac{1}{2\beta}\left[\sigma_{ey} + \sigma_t - \sqrt{\left(\sigma_{ey} + \sigma_t\right)^2 - 4\beta\sigma_{ey}\sigma_t}\right] \tag{15}$$

In accordance with AS/NZS 4673, the angle section columns subjected to concentric compression should be designed as beam-columns under eccentric compression introducing the additional bending moment of $P{\cdot}L/1000$ about the minor-principal axis that causes compressive stress in the leg tips. Unlike AISI-S100-16 [27], this requirement refers to both slender and non-slender angle sections. Therefore, the interaction formulae given by Eqs. (16) and (17) should be used:

$$\frac{N^*}{\phi_c N_s} + \frac{M_z^*}{\phi_b M_{bz}} \le 1.0 \tag{16}$$

$$\frac{N^*}{\phi_c N_c} + \frac{C_{mz} M_z^*}{\phi_b M_{bz} \alpha_{nz}} \le 1.0 \tag{17}$$

where N^* and M_z^* are the design axial compressive load and design bending moments about the z axis of the effective section (resulting from the initial design loading eccentricity of $L/1000$ and the effective centroid shift), respectively; N_s is the nominal member capacity of the member in compression; N_c is the nominal buckling capacity of the axially compressed member; M_{bz} is the nominal bending member capacity about the z axis (member lateral-torsional buckling moment resistance determined in accordance with Clause 3.3.3); α_{nz} is the amplification factor equal to $(1 - N^*/N_e)$ in in which N_e is the Euler buckling load about the minor-principal axis; C_{mz} is the equivalent uniform moment factor which is equal to unity for members with

constant first order bending moments along their length and for members whose ends are unrestrained; ϕ_c and ϕ_b are the strength reduction factors for compression and bending, respectively.

4. Finite element modelling and validation

The advanced and realistic numerical simulations of the experiments carried out on CFSS equal-leg angle columns [8] were performed using the ABAQUS FE software package [30]. The nominal section dimensions of specimens were 80 × 80 × 4 mm (leg width b × leg width b × thickness t) with a nominal internal corner radius r_i of 12 mm. The columns were divided into three test series with nominal lengths of 240 mm (labelled as ACF 80 × 80 × 4 – 240), 1000 mm (ACF 80 × 80 × 4 – 1000) and 2000 mm (ACF 80 × 80 × 4 – 2000). The geometrically and materially non-linear analysis (GMNIA) was developed as quasi-static with the dynamic explicit solver and the variable non-uniform mass scaling technique was used to shorten the computational time. Mass scaling with time increment of $5x10^{-6}$ *s* was used in the analyses. It should be emphasized that smaller values than the adopted scaling increment do not further change the columns' buckling responses and the ultimate load values obtained for the increment of $5x10^{-6}$ *s*. An appropriate smooth curve was adopted for amplitude functions in all loading steps to avoid large inertial forces in the quasi-static analysis. Quality of results was verified by matching input and output forces in a model for displacement-controlled failure loading. Linear matching curve with no oscillations proved that no inertia effects govern the results. An eigenvalue Linear Buckling Analysis (LBA) was previously employed to predict the critical buckling mode shapes used to model the distributions of the measured initial geometric imperfection and allow for a realistic incremental non-linear procedure. The numerical simulations cover all performed tests: stub column test on short length specimens, overall FTB and FB tests on intermediate length and long specimens, respectively. The aim was to reproduce the full load–deformation relationships, ultimate buckling loads and failures modes observed in the experiments.

The S4R shell elements with reduced integration and finite membrane strain were adopted to model the measured geometry of all specimens, as is customary for modelling thin-walled structures. A square mesh size with dimensions of the wall thickness t was chosen to discretise the flat and corner parts of the modelled angle section. To replicate the realistic supporting conditions of the pin-ended specimens in overall buckling tests, the measured geometry of steel loading plates attached to hardened steel knife-edges, employed in

experiments, together with top and bottom adjustable clamps were additionally modelled using four hexahedral solid elements C3D8R. Global element size of the plates was 5 mm, whereas the element size was reduced to 2 mm in the knife-edge zone. A uniform mesh with a size of 4 mm was employed to model both adjustable clamps. Contact conditions between the steel clamps and the loading plates were defined through tie constraints on the joining surfaces. The surface-to-surface general contact interaction was selected as the modelling approach, to account for the interactions between perimeter surfaces of specimen' end cross-sections, end adjustable clamps and loading plates, and also between the hardened steel knife-edges. The "hard contact" formulation of normal behaviour and the "penalty friction" formulation of tangential behaviour were used. The friction coefficient of 0.10 was assumed for all contact surfaces, except the frictionless conditions assumed between the top and bottom hardened knife surfaces as the special treatment with lubricant grease was applied in experiment. Two reference points were defined at the centroid of the top and bottom loading plates, which lie on the longitudinal axis passing through the centroids of the knife edges and the modelled test column. The external surfaces of loading plates that are kinematically coupled with reference points were fixed against all degrees of freedom except for the vertical displacement at the bottom loading plate where the failure loading was applied as controlled nodal displacement (set at the bottom reference point).

In order to simulate equivalent Boundary Conditions (BCs) at the ends of the model in stub-column tests, the end plates of the testing machine were modelled as a two-dimensional rigid body. The nodal surfaces of FE end plates were kinematically constrained to the central reference points having BCs that are fixed against all degrees of freedom except for the vertical displacement at the loaded edge. Typical geometry, boundary conditions and mesh are shown in Fig. 1.

Upon detailed examination of the response of the tested columns and obtained experimental data [8], it was observed that a small loading eccentricity about the minor-principal axis caused by adjustment errors of long specimens, was introduced in overall buckling tests. Based on the readings from the linear variable displacement transducers (LVDTs) and strain gauges (SGs), the initial loading eccentricity e_0 was determined as difference between the overall loading eccentricity, obtained in accordance with recommendations given in publication [31], and the initial mid-height global geometric imperfection amplitude about the minor

principal axis. It was found that initial eccentricity e_0 with values approximately in the range from 0.8 to 1.1 mm toward to the corner of the equal-leg angle section in the major-axis direction relative to the section centroid, was introduced in all repeated tests of long specimens (see Fig. 2). This eccentricity causes a distribution of tensile strains at the legs' tips and of compressive strains at the corner region. The realistic FE modelling allowed for a sophisticated analysis of the structural behaviour influenced by initial eccentricity and direct comparison with the experimental results.

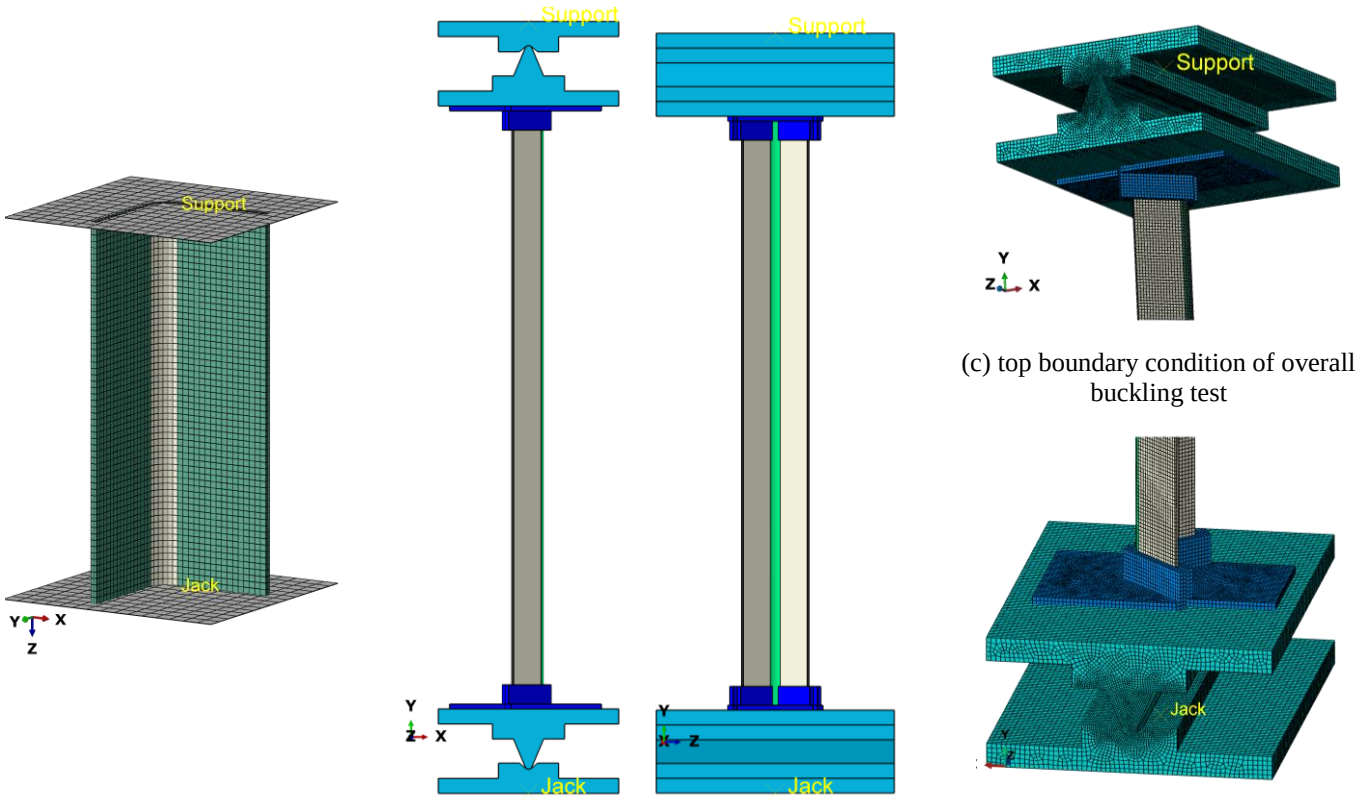

(a) stub-column test (b) overall buckling test

(c) top boundary condition of overall buckling test

(d) bottom boundary condition of overall buckling test

Fig. 1 Geometry, boundary conditions and mesh of the calibrated FE models [8].

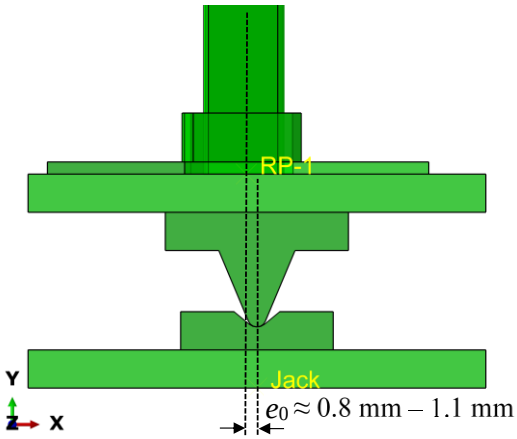

Fig. 2 Initial end eccentricity introduced in simulations of long column tests [8].

Nominal material properties of steel S275JR and S355N are used for end adjustable clamps and the hardened steel knife-edges in FE modelling, respectively, employing a linear elastic–perfectly plastic material model

with a nominal plateau slope. To account for the nonlinear material law, the measured stress–strain curves obtained via flat and corner tensile coupon tests on the lean duplex stainless steel grade EN 1.4162 (UNS S32101) were used to develop the material models of section' flat legs and corner, respectively. The material model of the corner part was confined to the corner region as it was considered that there are no significant strength increases beyond the curved portions in press-braked sections [32]. Isotropic plasticity with isotropic hardening was used with the Young's modulus values of 200 000 and 210 000 N/mm^2 respectively for stainless steel and all carbon steel grades, together with a Poisson's ratio v = 0.3. The nominal stress–strain curves were transformed to true stress–strain curves for input in the ABAQUS plasticity model. The nominal stress–strain curves used in FE material modelling are presented in Fig. 3.

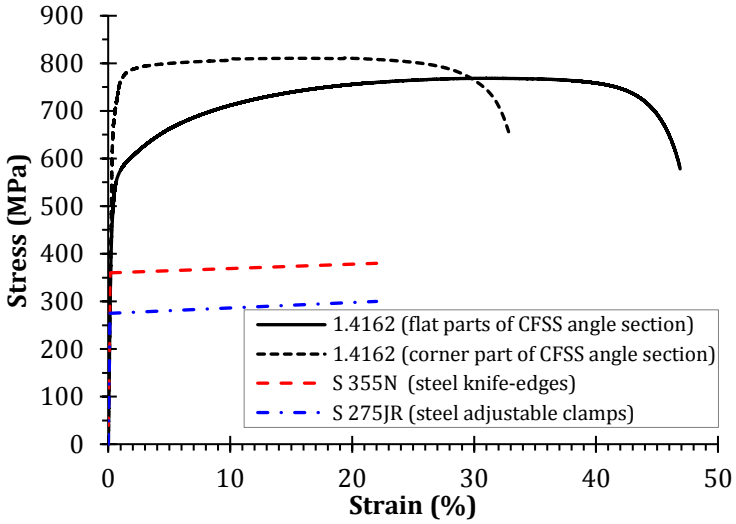

Fig. 3 Engineering stress–strain curves used in the FE models.

Considering the negligible influence of the residual stresses on cold-formed stainless steel members, and the inherent presence of through-thickness residual stresses in the measured material properties [33], [34], residual stresses were not explicitly modelled in the FE models.

The input geometric imperfections were linear combinations of sine wave functions which reflect the eigenmode shapes obtained via LBA performed on equivalent FE models with the same mesh. The imperfection shapes were taken in the form of the lowest global and local buckling modes. Two shape distributions of geometric imperfections were considered: a sine wave (bow) imperfection in the plane perpendicular to the minor-principal axis (flexural global mode) and a twist imperfection (local/torsional mode). The imperfection amplitudes matched the measured ones.

The validity, applicability and accuracy of FE modelling were assessed through a parallel and comparative analysis of the key experimental data and computational results: ultimate buckling loads and full load–strain and load–deflection curves. The numerical failure modes including local/torsional buckling and FTB for low and intermediate column slenderness, and minor-axis FB for high column slenderness match very well the experimental ones [8]. A qualitative comparisons of the ultimate buckling modes occurring in the column tests against the FE prediction for short, and for intermediate and long length columns are presented in Fig. 4 and Fig. 5, respectively. It can be seen that the buckling patterns in the experiment are very well reproduced by the FE modelling. Besides, distribution of axial stresses along the long length column with compressive yielding in corner region of the cross-section and tensile yielding in leg tips, which is clearly demonstrated in Fig. 5b, corresponds to stress distribution found in experiment [8].

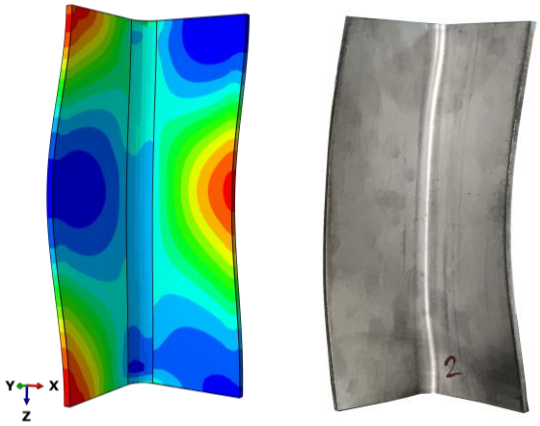

local/torsional buckling mode
ACF 80 × 80 × 4 – 240

Fig. 4 FE model and experimental [8] buckling pattern of equal-leg angle short column.

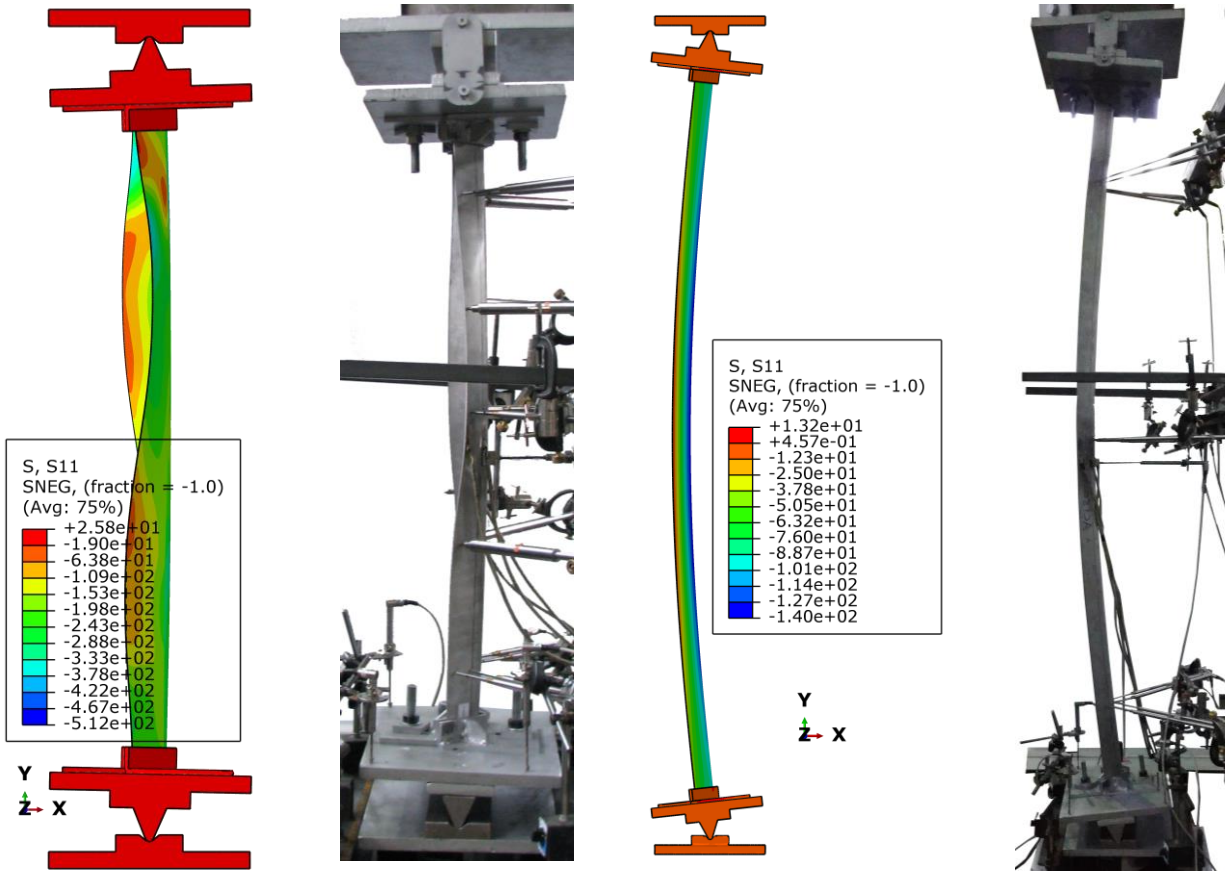

(a) FTB mode
ACF 80 × 80 × 4 – 1000

(b) FB mode
ACF 80 × 80 × 4 – 2000

Fig. 5 FE model and experimental [8] buckling pattern of equal-leg angle intermediate and long columns.

The comparisons between the experiment and FE models considering load versus end-shortening curves is shown in Fig. 6, whereas the comparisons of load versus longitudinal axial strain curves and load versus lateral deflection curves are shown in Fig. 7.

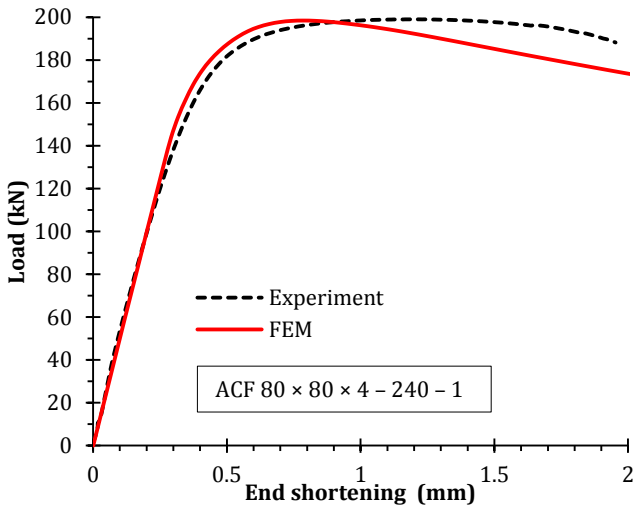

Load vs. end-shortening / short length column

Fig. 6 Comparison between experiments [8] and FE modelling results.

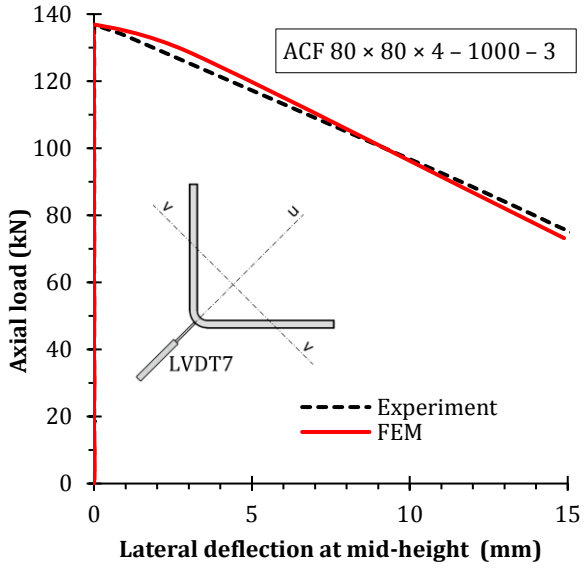

(a) Load vs. lateral deflection / intermediate length column

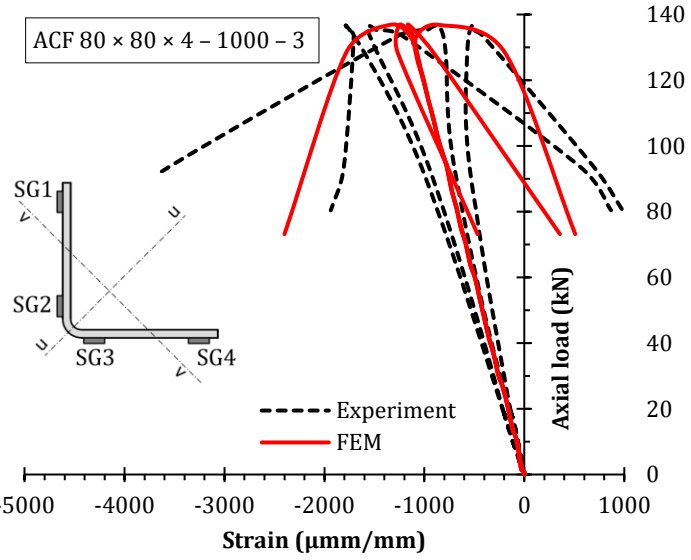

(b) Load vs. axial strains / intermediate length column

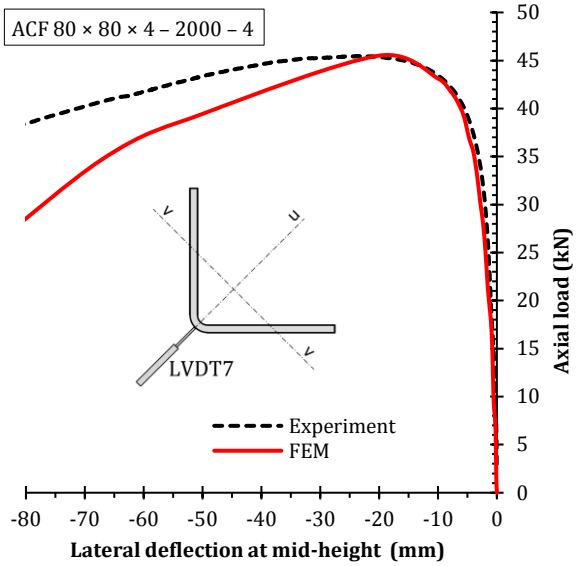

(c) Load vs. lateral deflection / long length column

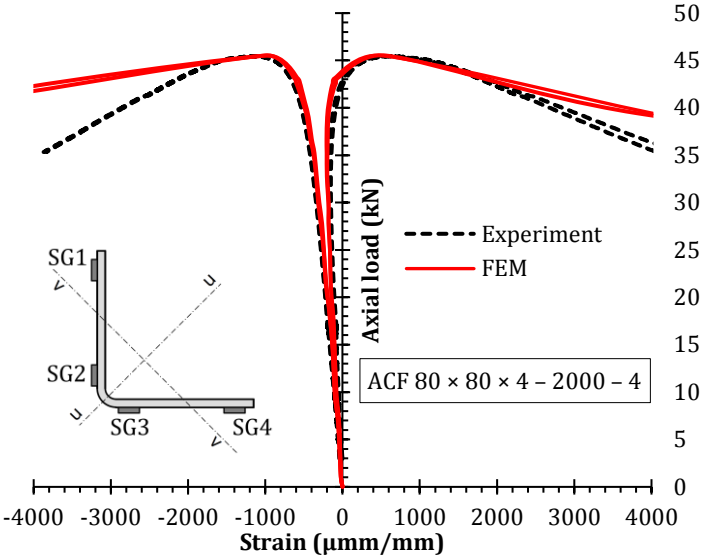

(d) Load vs. axial strains / long length column

Fig. 7 Comparison between experiments [8] and FE modelling results.

In the experiment by Dobrić et al. [8], the longitudinal axial strains were measured by SG1−SG4, placed in the positions of the cross-section at the mid-height of the specimens. The FE nodes corresponding to the same positions of SG1−SG4 were used to gain numerical longitudinal axial strains in FE models. The lateral deflections in the buckling plane perpendicular to the minor-principal axis were experimentally monitored by means of LVDT7 placed at the angle-section corner part at the mid-height of the specimens. The FE node corresponding to this LVDT was used to record numerical lateral deflections in FE models. Good matches, in terms of curves' shapes, initial stiffness, deformation capacity, ultimate resistance and post-buckling responses are evident.

FE models of the specimens in each tested series are additionally validated by comparing the numerically predicted ultimate buckling load $N_{b,u,FEM}$ with the averaged experimental values $N_{b,u,exp}$, as shown in Table 2. The ultimate loads are very well reproduced by the FE modelling, the average value of the FE model-to-experiments ultimate load ratio $N_{b,u,FEM}/N_{b,u,exp}$ equals 1.001 and the coefficient of variation (CoV) is 0.49%.

Table 2. Ultimate buckling load – experimental [8] and FE modelling results.

FE models / Specimens Designations as in [21]	Experiment					FE models	Ratio
	Repeated tests				Average value		
	1	2	3	4	$N_{b,u,exp}$	$N_{b,u,FEM}$	$N_{b,u,FEM}/N_{b,u,exp}$
ACF 80 × 80 × 4 – 240	199.0	198.2	203.7	-	200.3	199.5	0.996
ACF 80 × 80 × 4 – 1000	132.5	139.5	136.6	135.5	136.0	136.8	1.005
ACF 80 × 80 × 4 – 2000	44.3	45.8	46.8	45.5	45.6	45.8	1.004
Mean							1.001
CoV (%)							0.49

5. Imperfection sensitivity study

The permissible fabrication and erection tolerances prescribed in the appropriate codes are one of the most essential parameters in developing column design criteria. In this section, an imperfection sensitivity study is performed to assess the sensitivity of the column's compressive strengths to several combinations of imperfection modes and amplitudes. The imperfection sensitivity study focuses on pin-ended CFSS equal-leg angle columns with nominal cross-section dimensions 80 × 80 × 4 mm and different lengths covering the entire column slenderness range.

The geometry of FE models was developed based on nominal column dimensions using shell elements S4R with a global element size of 4 mm. Support and loading zones on the columns' ends are kinematically constrained to reference points in order to model the hinge-supported behaviour of the columns. Unlike realistic and explicit FE modelling of BCs of tested angle columns, presented in Section 4, in parametric studies the pin-ended supports are modelled with theoretical, idealized hinges, considering that the design procedures covering column buckling strengths usually involve the general case with this type of BCs. The reference points are set at the centroids of columns' end cross-sections. Failure loading is applied as displacement-controlled to a reference point in the loading zone. The material models developed on the basis of tensile flat and corner coupon tests performed on lean-duplex material (EN 1.4162), as in FE modelling (Section 4), were assigned to each FE model.

The superposition of initial geometric imperfections in the shape of the lowest minor-axis FB mode with an amplitude of $\delta_0 = \pm L/1000$ (L is the column length) and the lowest LB/TB mode is assigned to all FE models. The amplitude value of $L/1000$ of initial bow imperfections (out-of-straightness) corresponds to 75% of the maximum permitted imperfections for essential tolerances according to EN 1090-2 [35], as stated in Annex C of EN 1993-1-5 [22]. Two different magnitudes of the local/torsional imperfections were considered: $\omega_0 = \pm t/10$ (t is the leg thickness) in agreement with [12], [13], and $\omega_0 = \pm b/50$ (b is the leg width) based on Annex C of EN 1993-1-5 [22]. Considering that the sign of initial imperfections is not explicitly defined in Technical requirements [35], and it is not obvious without previous measurements, both directions of imperfection distributions were employed in the GMNIA: in the positive directions related to deformed buckling shapes of FE models obtained in the LBA and in negative directions that are opposite from the directions of the deformed buckling shapes of FE models in the LBA. The positive sign of local imperfections corresponds to cross-section rotation in the clockwise direction (see Fig. 8a), whereas the positive sign of global imperfections corresponds to the deformed column which bends out towards the leg tips of the angle section (tensile yielding in the leg tips), see Fig. 8b.

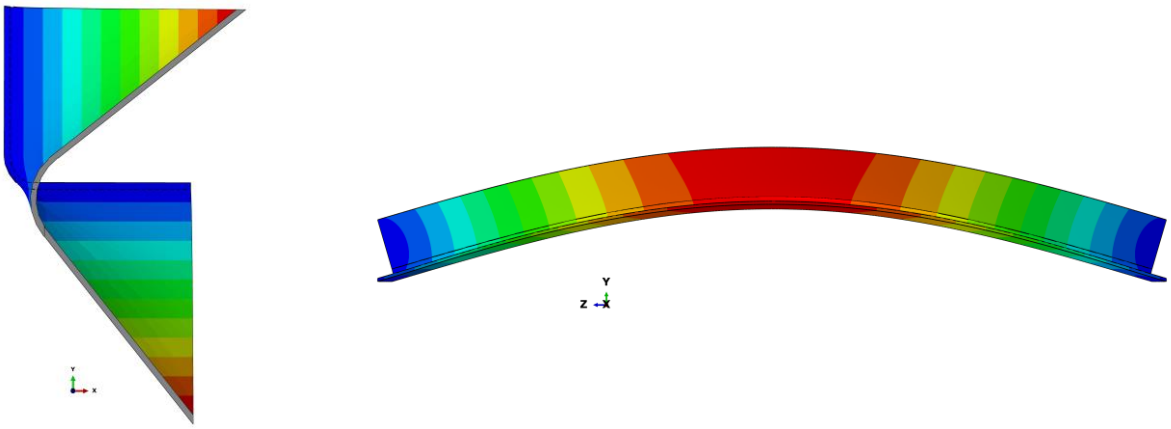

(a) local/torsional imperfection (b) global bow imperfections

Fig. 8 Distribution patterns of initial geometric imperfections with positive sign.

The compressive capacities of imperfect FE models ($N_{b,u,imperfect}$) are compared with compressive capacities of the equivalent initially straight columns ($N_{b,u,straight}$).

Table 3 quantifies the decrease of column buckling resistance of initially straight columns caused by influences of combined actions of geometric imperfections (GI) accounting for the change of distribution sign.

Table 3. Quantification of the initial GI influences on the FE ultimate buckling loads.

		$N_{b,u,imperfect}$ / $N_{b,u,straight}$							
FE models / Designations as in [21]	Non-dimensional slenderness $\bar{\lambda}_v$	+*t*/10 & +*L* /1000	+*t*/10 & -*L* /1000	-*t*/10 & +*L* /1000	-*t*/10 & -*L* /1000	+*b*/50 & +*L* /1000	+*b*/50 & -*L* /1000	-*b*/50 & +*L* /1000	-*b*/50 & -*L* /1000
ACF 80 × 80 × 4 – 300	0.236	0.852	0.863	0.852	0.863	0.741	0.751	0.741	0.751
ACF 80 × 80 × 4 – 400	0.314	0.822	0.815	0.822	0.815	0.712	0.705	0.712	0.706
ACF 80 × 80 × 4 – 500	0.393	0.813	0.797	0.813	0.797	0.699	0.687	0.699	0.688
ACF 80 × 80 × 4 – 600	0.471	0.799	0.769	0.799	0.770	0.692	0.672	0.692	0.672
ACF 80 × 80 × 4 – 700	0.550	0.789	0.748	0.788	0.747	0.692	0.653	0.692	0.653
ACF 80 × 80 × 4 – 800	0.629	0.816	0.752	0.816	0.752	0.707	0.658	0.707	0.659
ACF 80 × 80 × 4 – 900	0.707	0.813	0.726	0.812	0.726	0.705	0.639	0.705	0.640
ACF 80 × 80 × 4 – 1000	0.786	0.822	0.715	0.823	0.715	0.713	0.632	0.713	0.632
ACF 80 × 80 × 4 – 1200	0.943	0.858	0.691	0.860	0.690	0.744	0.608	0.745	0.608
ACF 80 × 80 × 4 – 1400	1.100	0.747	0.647	0.746	0.647	0.758	0.587	0.756	0.587
ACF 80 × 80 × 4 – 1500	1.179	0.683	0.620	0.682	0.620	0.687	0.568	0.686	0.568
ACF 80 × 80 × 4 – 1600	1.257	0.655	0.607	0.656	0.607	0.656	0.571	0.657	0.571
ACF 80 × 80 × 4 – 1800	1.414	0.613	0.579	0.613	0.579	0.613	0.561	0.613	0.561
ACF 80 × 80 × 4 – 2000	1.571	0.566	0.551	0.566	0.551	0.566	0.542	0.566	0.542
ACF 80 × 80 × 4 – 2200	1.729	0.519	0.515	0.519	0.519	0.519	0.513	0.519	0.513
ACF 80 × 80 × 4 – 2400	1.886	0.477	0.476	0.477	0.476	0.477	0.475	0.477	0.475
ACF 80 × 80 × 4 – 2500	1.964	0.458	0.457	0.458	0.457	0.458	0.457	0.458	0.457
ACF 80 × 80 × 4 – 2600	2.043	0.441	0.440	0.441	0.440	0.441	0.440	0.441	0.440
ACF 80 × 80 × 4 – 2800	2.200	0.402	0.401	0.402	0.401	0.401	0.401	0.401	0.402
ACF 80 × 80 × 4 – 3000	2.357	0.372	0.372	0.372	0.372	0.372	0.372	0.372	0.372
ACF 80 × 80 × 4 – 3200	2.514	0.343	0.343	0.343	0.343	0.342	0.342	0.342	0.343
ACF 80 × 80 × 4 – 3400	2.671	0.320	0.320	0.320	0.320	0.319	0.320	0.319	0.320

A brief analysis of the obtained results is presented as below.

- The torsional imperfection with an amplitude of $b/50$ more adversely affects column buckling resistance in comparison with an equivalent imperfection with an amplitude of $t/10$ in the low and intermediate slenderness range up to $\bar{\lambda}_v = 1.571$. In the high slenderness range, the torsional imperfection does not have any noticeable effect on buckling behaviour of CFSS angle column. The ultimate structural response of the column does not depend on the torsional amplitude sign.
- The combined effects of the bow imperfection with amplitude of $-L/1000$ (column bents out towards the cross-section corner causing compressive yielding in leg tips) and torsional imperfection with amplitude of $+b/50$ reduce the ultimate strength of a perfectly straight column from 25% in the low slenderness range ($\bar{\lambda}_v = 0.236$) up to 68% in the high slenderness range ($\bar{\lambda}_v = 2.671$). The results in Table 3 indicate that the presence of such imperfections ($+b/50$ and $-L/1000$) leads to the lowest values of ultimate buckling loads.

6. Numerical parametric study

The validated FE modelling was used to perform a wide-ranging parametric study on the compressive capacity of CFSS equal-leg angle columns and to develop a framework for their reliability-based design. To predict cross-section resistances and assess plateau length of buckling curves, fixed-ended short length columns were involved in the study. The length of these columns was set equal to three times the leg width. Additionally, pin-ended columns were studied to predict minor-axis FB and FTB capacity of intermediate length and long columns, respectively and to derive a series of buckling curves for their design.

In total, 27 different equal-leg angle section dimensions were selected providing both slender and non-slender cross-sectional behaviour. The maximum width-to-thickness ratios of angle legs satisfy the conditions of Table 5.1 of EN 1993-1-3 [24]. Table 4 lists geometric properties of angle columns considered in the present study.

Table 4. Cross-section geometries and lengths of CFSS angle columns included in the present study.

Equal-leg angle section	Column length L (mm)	Leg width b (mm)	Thickness t (mm)	Internal radius r_i (mm)
ACF 50 × 50 × 2	150–2200	50	2	4
ACF 50 × 50 × 4	150–2200	50	4	8
ACF 50 × 50 × 5	150–1500	50	5	10
ACF 60 × 60 × 2	180–2400	60	2	4
ACF 60 × 60 × 3	180	60	3	6
ACF 60 × 60 × 4	180–2800	60	4	8
ACF 60 × 60 × 6	180–2000	60	6	12
ACF 65 × 65 × 2.5	195	65	2.5	5
ACF 65 × 65 × 3	195	65	3	6
ACF 70 × 70 × 6	210–2600	70	6	12
ACF 70 × 70 × 8	210–2200	70	8	16
ACF 70 × 70 × 10	210–2200	70	10	20
ACF 75 × 75 × 3	225	75	3	6
ACF 75 × 75 × 3.5	225	75	3.5	7
ACF 80 × 80 × 4	240–3200	80	4	12
ACF 80 × 80 × 6	240–3200	80	6	12
ACF 80 × 80 × 10	240–2500	80	10	20
ACF 90 × 90 × 4	270	90	4	8
ACF 100 × 100 × 4	300–3600	100	4	8
ACF 100 × 100 × 6	300–3600	100	6	12
ACF 100 × 100 × 8	100–3300	100	8	16
ACF 150 × 150 × 4	450–3000	150	4	8
ACF 150 × 150 × 6	450–3800	150	6	12
ACF 150 × 150 × 8	450–4000	150	8	16
ACF 200 × 200 × 4	600–3300	200	4	8
ACF 200 × 200 × 6	600–3300	200	6	12
ACF 200 × 200 × 8	600–3300	200	8	16

The influence of material nonlinearity on column ultimate strength was thoroughly analysed for three primary alloys: austenitic, ferritic and duplex stainless steel. It was assumed that press-braked equal-leg angle columns may be produced both from cold-rolled and hot-rolled strips. Thus, the numerical material models were developed based on mechanical properties obtained by Lecce's tensile tests performed on the coupons extracted from the strips in hot-rolled condition EN 1.4301 [36], Dobrić's tests in cold-rolled condition EN 1.4301 [4] and hot-rolled condition EN 1.4162 [8] and Rossi's tests in the cold-rolled condition EN 1.4003 [37]. Full stress-strain experimental curves (flat and corner coupons) were used for austenitic (cold-rolled condition) [4] and duplex alloys [8], whereas the modified Ramberg-Osgood analytical model [38] (in the absence of experimental curves) was employed to model the material response for austenitic (hot-rolled condition) [36] and ferritic alloys [37]. Rossi's predictive model [32] was used to account for the strain-hardening effects in the cross-section corner region caused by the press-braking process. In the subsequent sections of this paper, the terms "HR" and "CR" are used to denote CFSS angle columns produced from hot-rolled and cold-rolled strips, respectively.

Table 5 and Table 6 provide the material parameters included in the FE models for the flats and corners of the studied cross-sections: the yield strength f_y taken as the 0.2 % proof strength, the ultimate tensile strength f_u, the strain corresponding to the ultimate tensile strength ε_u and the strain hardening parameters n and m.

Table 5. Key material properties of flat cross-section parts adopted in the FE models.

Stainless steel grade / Source	f_y (N/mm^2)	f_u (N/mm^2)	ε_u (%)	Strain hardening parameters	
				n	m
EN 1.4003 / [37]	337	614	29	13.5	2.0
EN 1.4162 / [8]	517	768	31	7.9	3.0
EN 1.4301 / [36]	251	703	57	5.0	2.2
EN 1.4301 / [4]	307	634	53	6.3	2.2

Table 6. Key material properties of corner cross-section parts adopted in the FE models.

Stainless steel grade / Source	f_y (N/mm^2)	f_u (N/mm^2)	ε_u (%)	Strain hardening parameters	
				n	m
EN 1.4003 / [37]	525	624	10	13.5	3.4
EN 1.4162 / [8]	703	823	17	11	13.1
EN 1.4301 / [36]	570	784	16	5.0	3.0
EN 1.4301 / [4]	458	680	37	4.9	2.5

The initial geometric imperfections in the form of buckling mode shapes were introduced in each FE model. The local/torsional imperfection with an amplitude of $+b/50$ was used to investigate local cross-section instability. The pattern, including a superposition of the local/torsional imperfection with an amplitude of $+b/50$ and a bow (sine wave) imperfection with a magnitude of $-L/1000$, was used to assess the global stability of angle columns.

7. Comparison with European and Australian design resistances

A comparison of the generated numerical data with the design data determined according to the European and Australian/New Zealand standards is presented in this section. The numerical results were carefully considered to clearly identify the failure modes. The numerical failure mode governed by dominant LB/TB, FTB or minor-axis FB was selected to evaluate the corresponding design failure load. The test data on compressed cold-formed stainless steel equal-leg angle columns collected from the literature [7], [8] are also included in the comparisons. The procedure described in Clause 5.2.3, EN 1993-1-4 [20], and the Clauses 2.2 and 2.3, AS/NZS 4673 [21] were followed to obtain the effective areas of the slender cross-sections (Class 4). According to AS/NZS 4673 [21], the minor-axis column buckling strengths were calculated using the explicit approach that accounts for material nonlinearities by introducing the parameters α, β, λ_0 and λ_1 (as provided in Table 1). To evaluate the influence of the shift in neutral axis resulting from the local buckling, the data points related to slender cross-sections were selected and reassessed based on interaction formulae

stated in Clause 5.5 [20] and Clause 3.5 [21], respectively. The effective centroid shift was determined as the distance between centroids of a full (unreduced) and effective equal-leg angle section. The direction of the predicted shift in the angle section (along the major-principal axis) leads to a secondary minor-axis bending moment with no secondary major axis bending moment. A shift of the effective centroid towards the section corner causes bending towards the corner. The additional loading eccentricity of $L/1000$ to the minor-principal axis was considered both for slender and non-slender sections, in accordance with AS/NZS 4673 [21]. Both codified approaches involved the use of an average or weighted average cross-section along the column length for calculating the ultimate buckling strengths.

Table 7 contains a summary of data gained from numerical simulations of short columns, in which $\sigma_{lb,FE} / f_{ya}$ is the local buckling stress-to-enhanced average yield ratio, $\sigma_{lb,FE}$ is the LB stress obtained as the ultimate load-to-nominal gross cross-section area ratio of each FE model and f_{ya} is an enhanced average yield strength which accounts for cold working in press-braked sections, obtained in accordance with the proposal by Rossi et al. [32]. In Fig. 9, the FE and test ultimate loads for short columns are normalised with cross-section yield loads taken as the product of cross-section area and enhanced average yield strength, and plotted against the non-dimensional column slenderness ratio for minor-axis FB, $\bar{\lambda}_v$. In addition, Fig. 10 and Fig. 11 show the graphical comparisons of the European buckling curves *b* (α = 0.34), *c* (α = 0.49) and *d* (α = 0.76) in conjunction with a limiting non-dimensional slenderness $\bar{\lambda}_0$ = 0.2 with the FE and test ultimate loads normalised by the cross-section yield loads, for dominant minor-axis FB and FTB failure modes, respectively. The data points are plotted against the non-dimensional column slenderness ratio (minor-axis FB slenderness ratio $\bar{\lambda}_v$ for minor-axis FB failures, and FT slenderness ratio $\bar{\lambda}_{FT}$ for FTB failures). The EN 1993-1-4 [20] buckling curve for cold-formed sections, with the imperfection factor α = 0.49 and $\bar{\lambda}_0$ = 0.4 is also depicted in Fig. 10. The results for columns with both slender and non-slender sections are presented in these three graphs using different colour coding for each stainless steel family. Note that codified buckling curves depict predicted compressive strength of axially loaded columns without consideration of the neutral axis shift in the case of slender sections.

Table 7. Assessment of cross-section buckling modes.

FE model	Austenitic CF			Austenitic HR			Duplex			Ferritc		
	$\sigma_{lb,FE}$ / f_{ya}	Cross-section classification		$\sigma_{lb,FE}$ / f_{ya}	Cross-section classification		$\sigma_{lb,FE}$ / f_{ya}	Cross-section classification		$\sigma_{lb,FE}$ / f_{ya}	Cross-section classification	
		EN 1993-1-4	AS/NZS 4673		EN 1993-1-4	AS/NZS 4673		EN 1993-1-4	AS/NZS 4673		EN 1993-1-4	AS/NZS 4673
ACF 50 × 50 × 2 – 150	0.60	Slender	Slender	0.64	Slender	Slender	0.58	Slender	Slender	0.61	Slender	Slender
ACF 50 × 50 × 4 – 150	0.90	Slender	Slender	0.92	Non-slender	Slender	0.88	Slender	Slender	0.88	Slender	Slender
ACF 50 × 50 × 5 – 150	0.99	Non-slender	Non-slender	1.01	Non-slender	Non-slender	0.99	Slender	Slender	0.96	Non-slender	Non-slender
ACF 60 × 60 × 2 – 180	0.54	Slender	Slender	0.58	Slender	Slender	0.52	Slender	Slender	0.56	Slender	Slender
ACF 60 × 60 × 4 – 180	0.81	Slender	Slender	0.84	Slender	Slender	0.78	Slender	Slender	0.81	Slender	Slender
ACF 60 × 60 × 6 – 180	0.99	Non-slender	Non-slender	1.01	Non-slender	Non-slender	0.98	Slender	Slender	0.96	Non-slender	Non-slender
ACF 70 × 70 × 6 – 210	0.93	Non-slender	Slender	0.95	Non-slender	Slender	0.91	Slender	Slender	0.91	Slender	Slender
ACF 70 × 70 × 8 – 210	1.04	Non-slender	Non-slender	1.06	Non-slender	Non-slender	1.03	Non-slender	Non-slender	0.99	Non-slender	Non-slender
ACF 70 × 70 × 10 – 210	1.09	Non-slender	Non-slender	1.12	Non-slender	Non-slender	1.07	Non-slender	Non-slender	1.04	Non-slender	Non-slender
ACF 80 × 80 × 4 – 240	0.69	Slender	Slender	0.76	Slender	Slender	0.66	Slender	Slender	0.70	Slender	Slender
ACF 80 × 80 × 6 – 240	0.87	Slender	Slender	0.89	Slender	Slender	0.84	Slender	Slender	0.86	Slender	Slender
ACF 80 × 80 × 10 – 240	1.06	Non-slender	Non-slender	1.08	Non-slender	Non-slender	1.05	Non-slender	Non-slender	1.01	Non-slender	Non-slender
ACF 100 × 100 × 4 – 300	0.60	Slender	Slender	0.65	Slender	Slender	0.58	Slender	Slender	0.62	Slender	Slender
ACF 100 × 100 × 6 – 300	0.77	Slender	Slender	0.81	Slender	Slender	0.73	Slender	Slender	0.77	Slender	Slender
ACF 100 × 100 × 8 – 300	0.89	Slender	Slender	0.87	Non-slender	Slender	0.87	Slender	Slender	0.87	Slender	Slender
ACF 150 × 150 × 4 – 450	0.47	Slender	Slender	0.51	Slender	Slender	0.44	Slender	Slender	0.49	Slender	Slender
ACF 150 × 150 × 6 – 450	0.60	Slender	Slender	0.64	Slender	Slender	0.58	Slender	Slender	0.61	Slender	Slender
ACF 150 × 150 × 8 – 450	0.70	Slender	Slender	0.74	Slender	Slender	0.68	Slender	Slender	0.72	Slender	Slender
ACF 200 × 200 × 4 – 600	0.39	Slender	Slender	0.42	Slender	Slender	0.35	Slender	Slender	0.41	Slender	Slender
ACF 200 × 200 × 6 – 600	0.51	Slender	Slender	0.55	Slender	Slender	0.48	Slender	Slender	0.52	Slender	Slender
ACF 200 × 200 × 8 – 600	0.60	Slender	Slender	0.64	Slender	Slender	0.57	Slender	Slender	0.61	Slender	Slender
ACF 60 × 60 × 3 – 180	0.68	Slender	Slender	0.72	Slender	Slender	0.66	Slender	Slender	0.70	Slender	Slender
ACF 65 × 65 × 2.5 – 195	0.59	Slender	Slender	0.63	Slender	Slender	0.57	Slender	Slender	0.60	Slender	Slender
ACF 65 × 65 × 3 – 195	0.65	Slender	Slender	0.69	Slender	Slender	0.63	Slender	Slender	0.66	Slender	Slender
ACF 75 × 75 × 3 – 225	0.60	Slender	Slender	0.64	Slender	Slender	0.58	Slender	Slender	0.61	Slender	Slender
ACF 75 × 75 × 3. 5– 225	0.65	Slender	Slender	0.69	Slender	Slender	0.63	Slender	Slender	0.67	Slender	Slender
ACF 90 × 90 × 4 – 270	0.64	Slender	Slender	0.68	Slender	Slender	0.61	Slender	Slender	0.65	Slender	Slender

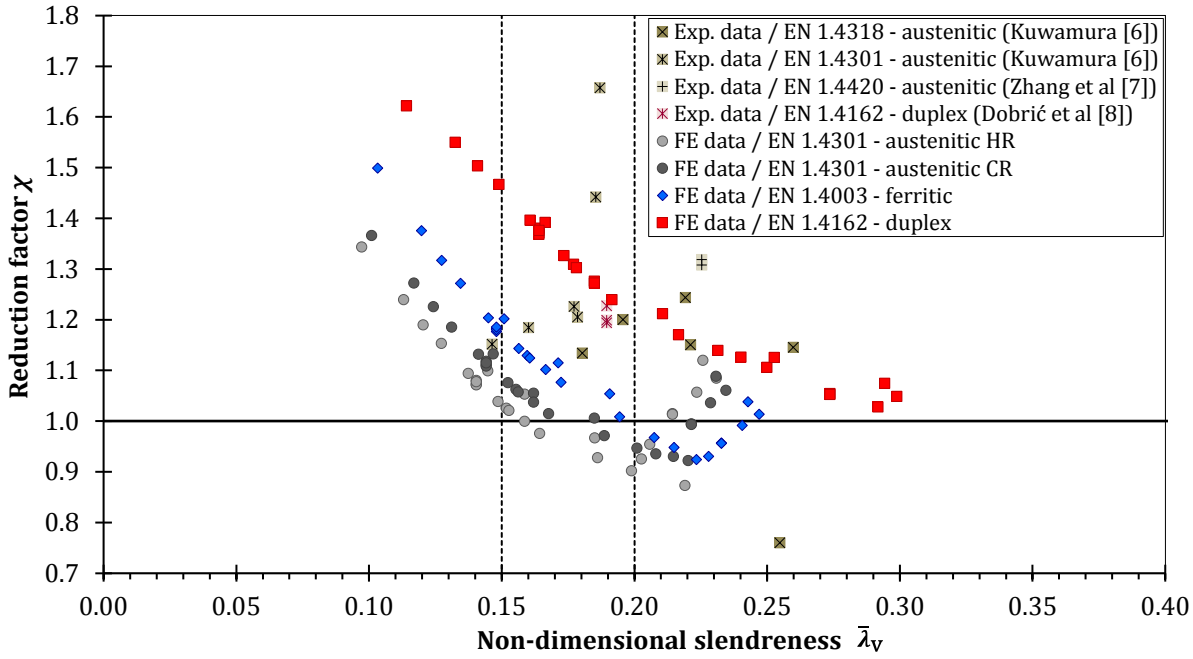

Fig. 9 Assessment of length plateau of design buckling curve.

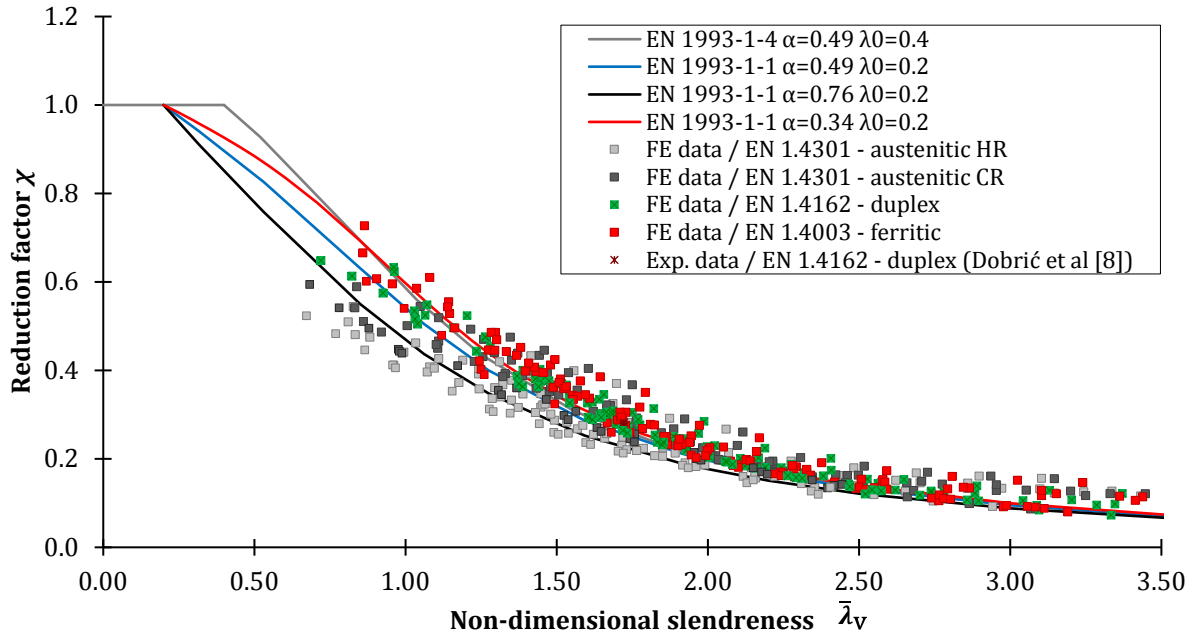

Fig. 10 Comparison between normalised FE & test results and EN 1993-1-4 for minor-axis FB.

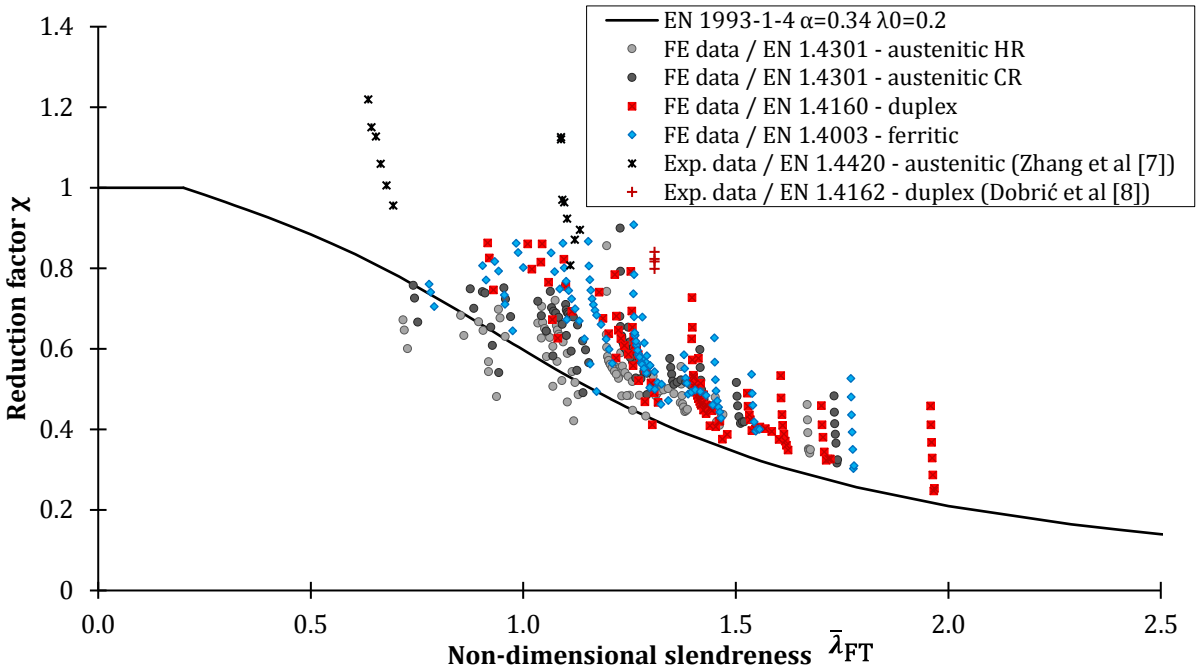

Fig. 11 Comparison between normalised FE & test results and EN 1993-1-4 curves for FTB.

In addition, Table 8 provides accuracy assessment of each codified procedure considering the FE & test-to-predicted ratios $N_{b,u}/N_{b,u,pred}$ per grade and per cross-section class. The design predictions for slender sections (Class 4), which are included in resistance ratios listed in Table 8, were obtained using interaction Eqs. (7) and (17) for Eurocode and AS/NZS, respectively. In the case of AS/NZS dataset, the parameters provided in Table 1 are denoted with the subscript AS/NZS: $\alpha_{AS/NZS}$ and $\lambda_{0,AS/NZS}$.

Table 8. Comparison between FE & test data and design data (an average value higher than 1.0 could indicate safe predictions).

Grade		Code	Data no.	$N_{b,u}/N_{b,u,pred}$	
			$\overline{\lambda}_0 > 0.2$	Mean	CoV (%)
EN 1993-1-4 / minor-axis FB (& minor-axis bending)					
Austenitic	Non-slender – Class 3	$\alpha = 0.76$ $\overline{\lambda}_0 = 0.2$	98	1.181	27.1
	Slender – Class 4	$\alpha = 0.76$ $\overline{\lambda}_0 = 0.2$ & Eq. (7)	193	1.910	40.6
Duplex	Non-slender – Class 3	$\alpha = 0.49$ $\overline{\lambda}_0 = 0.2$	21	1.007	2.6
	Slender – Class 4	$\alpha = 0.49$ $\overline{\lambda}_0 = 0.2$ & Eq. (7)	119	2.054	39.2
Ferritic	Non-slender – Class 3	$\alpha = 0.49$ $\overline{\lambda}_0 = 0.2$	49	1.159	21.1
	Slender – Class 4	$\alpha = 0.49$ $\overline{\lambda}_0 = 0.2$ & Eq. (7)	85	1.953	38.4
EN 1993-1-4 / FTB & minor-axis bending					
Austenitic	Slender – Class 4	$\alpha = 0.34$ $\overline{\lambda}_0 = 0.2$ & Eq. (7)	212	2.892	32.7
Duplex	Slender – Class 4	$\alpha = 0.34$ $\overline{\lambda}_0 = 0.2$ & Eq. (7)	104	3.779	28.2
Ferritic	Slender – Class 4	$\alpha = 0.34$ $\overline{\lambda}_0 = 0.2$ & Eq. (7)	104	3.373	29.7
AS/NZS 4673 / minor-axis FB & minor-axis bending					
Austenitic	Non-slender	$\alpha_{AS/NZS} = 1.59$ $\lambda_{0,AS/NZS} = 0.55$	98	1.157	22.9
	Slender	$\alpha_{AS/NZS} = 1.59$ $\lambda_{0,AS/NZS} = 0.55$ & Eq. (17)	193	1.630	30.3
Duplex	Non-slender	$\alpha_{AS/NZS} = 1.16$ $\lambda_{0,AS/NZS} = 0.65$	21	0.967	2.9
	Slender	$\alpha_{AS/NZS} = 1.16$ $\lambda_{0,AS/NZS} = 0.65$ & Eq. (17)	119	1.569	26.3
Ferritic	Non-slender	$\alpha_{AS/NZS} = 0.94$ $\lambda_{0,AS/NZS} = 0.56$	49	1.134	19.4
	Slender	$\alpha_{AS/NZS} = 0.94$ $\lambda_{0,AS/NZS} = 0.56$ & Eq. (17)	85	1.597	26.8
AS/NZS 4673 / FTB & minor-axis bending					
Austenitic	Slender	Eqs. (15) & (17)	212	2.100	29.7
Duplex	Slender	Eqs. (15) & (17)	104	2.470	24.7
Ferritic	Slender	Eqs. (15) & (17)	104	2.360	26.9

The points, representing pairs of corresponding FE & test data ($N_{b,u}$) and design data ($N_{b,u,pred}$), related to minor-axis FB and FTB are respectively plotted in Fig. 12 and Fig. 13, including both slender and non-slender cross-sections and all analysed stainless steel grades.

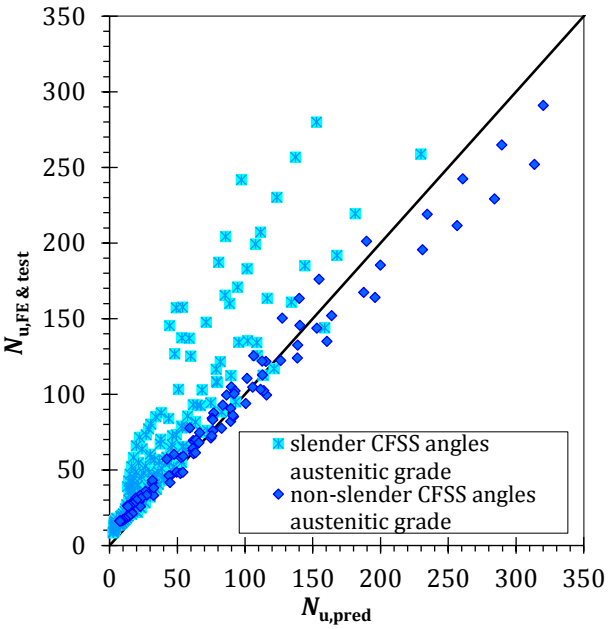

(a) EN 1993-1-4 / austenitic grade
$\alpha = 0.76$ $\bar{\lambda}_0 = 0.2$ & Eq. (7)

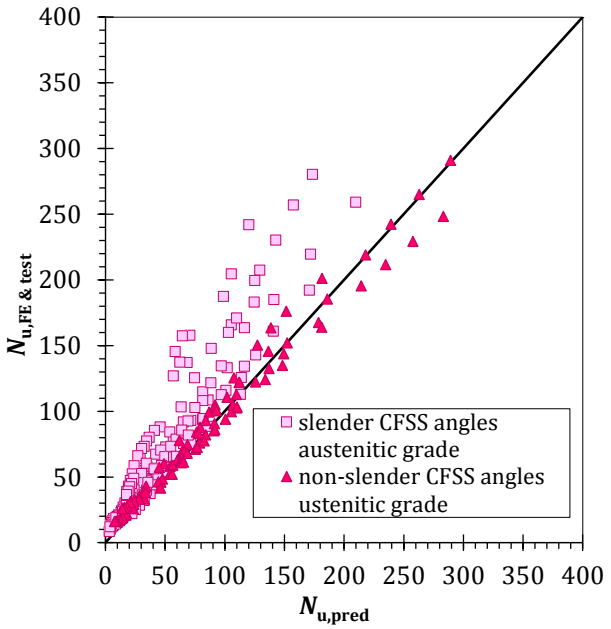

(b) AS/NZS 4673 / austenitic grade
$\alpha_{AS/NZS} = 1.59$ $\lambda_{0,AS/NZS} = 0.55$ & Eq. (17)

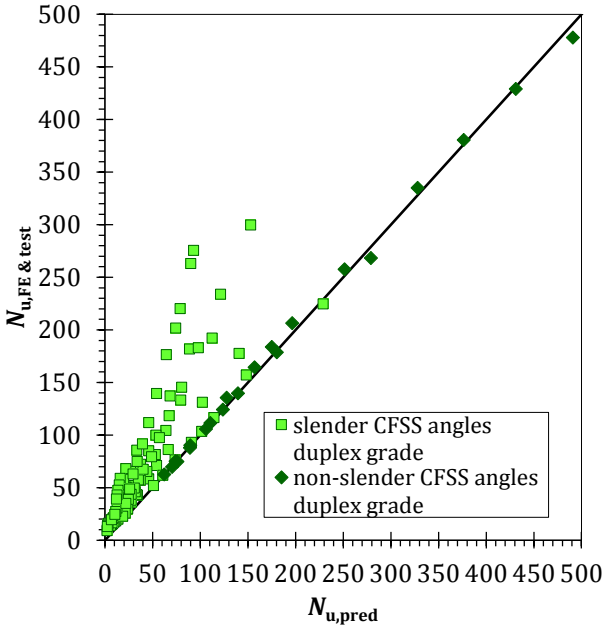

(c) EN 1993-1-4 / duplex grade
$\alpha = 0.49$ $\bar{\lambda}_0 = 0.2$ & Eq. (7)

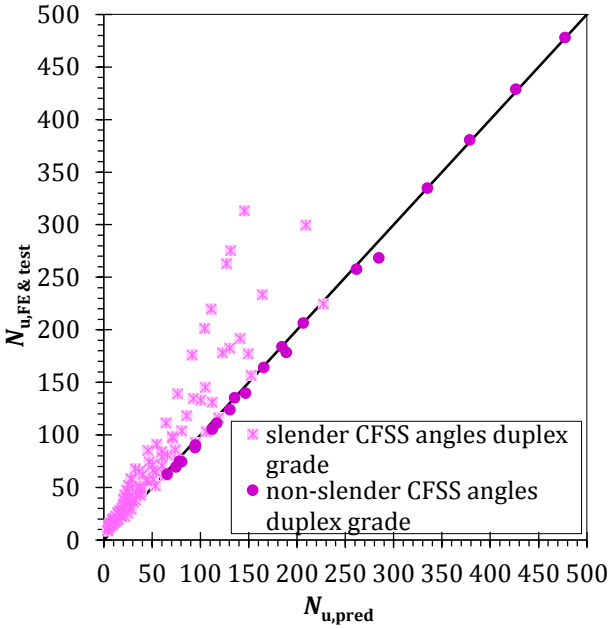

(d) AS/NZS 4673 / duplex grade
$\alpha_{AS/NZS} = 1.16$ $\lambda_{0,AS/NZS} = 0.65$ & Eq. (17)

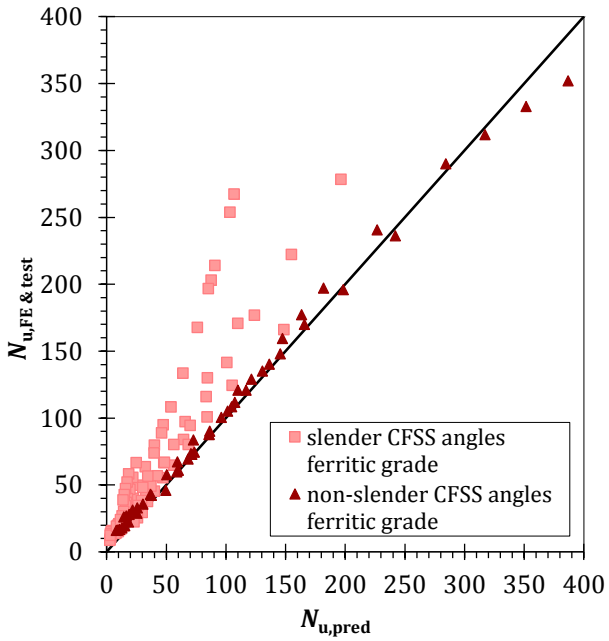

(e) EN 1993-1-4 / ferritic grade
$\alpha = 0.49$ $\bar{\lambda}_0 = 0.2$ & Eq. (7)

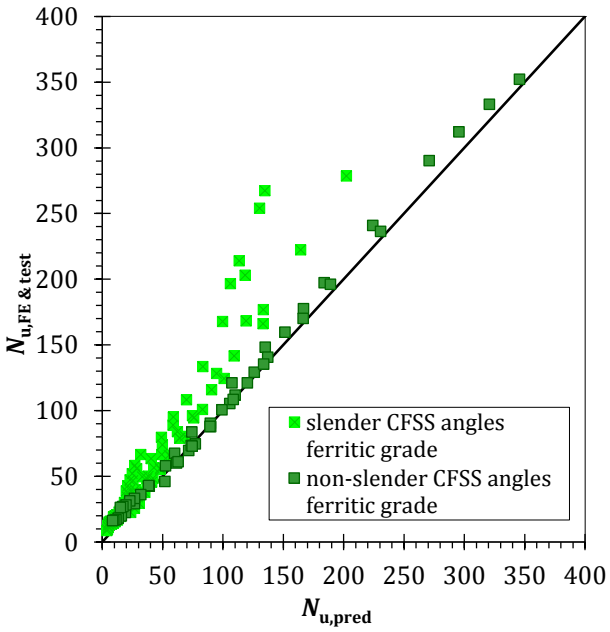

(f) AS/NZS 4673 / ferritic grade
$\alpha_{AS/NZS} = 0.94$ $\lambda_{0,AS/NZS} = 0.56$ & Eq. (17)

Fig. 12 Comparison of FE & test resistance with design resistance predictions for minor-axis FB.

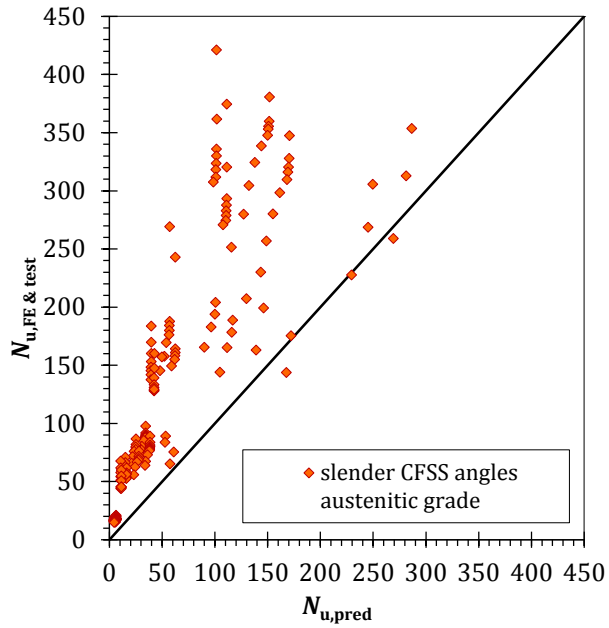

(a) EN 1993-1-4 / austenitic grade
$\alpha = 0.34$ $\bar{\lambda}_0 = 0.2$ & Eq. (7)

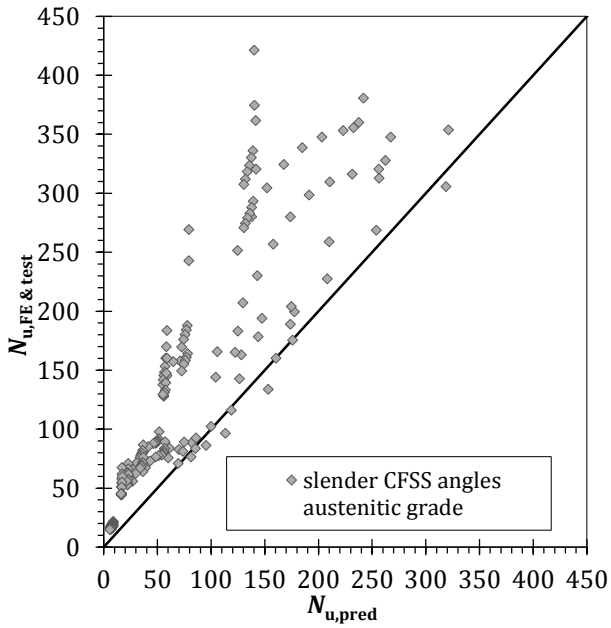

(b) AS/NZS 4673 / austenitic grade
Eqs. (15) & (17)

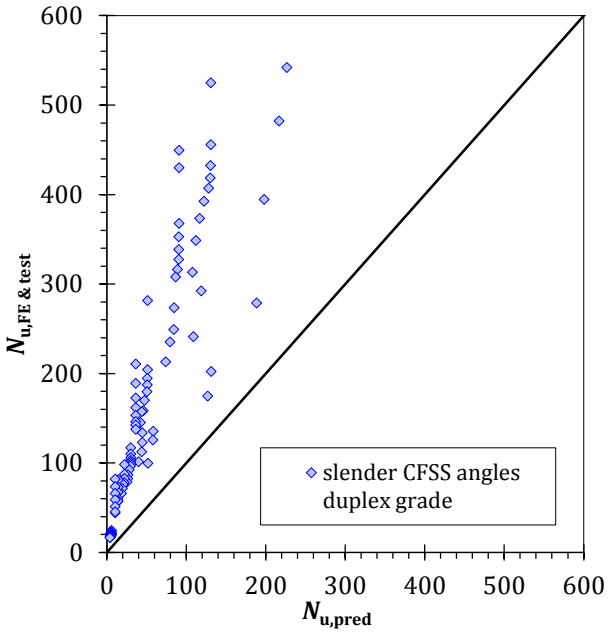

(c) EN 1993-1-4 / duplex grade
$\alpha = 0.49$ $\bar{\lambda}_0 = 0.2$ & Eq. (7)

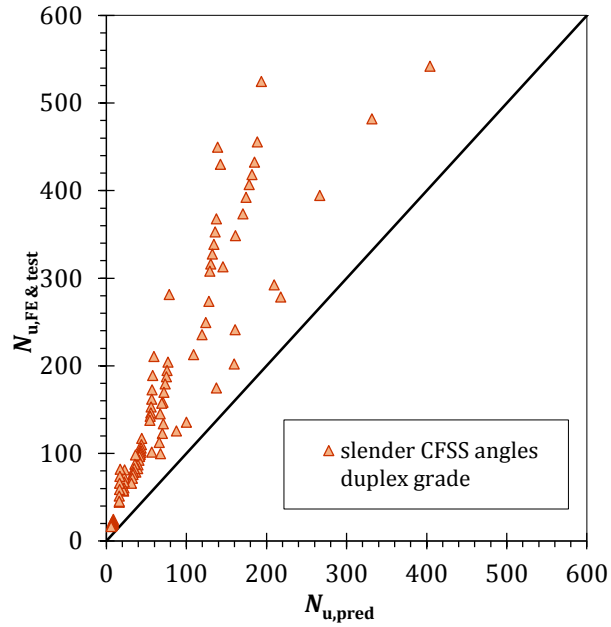

(d) AS/NZS 4673 / duplex grade
Eqs. (15) & (17)

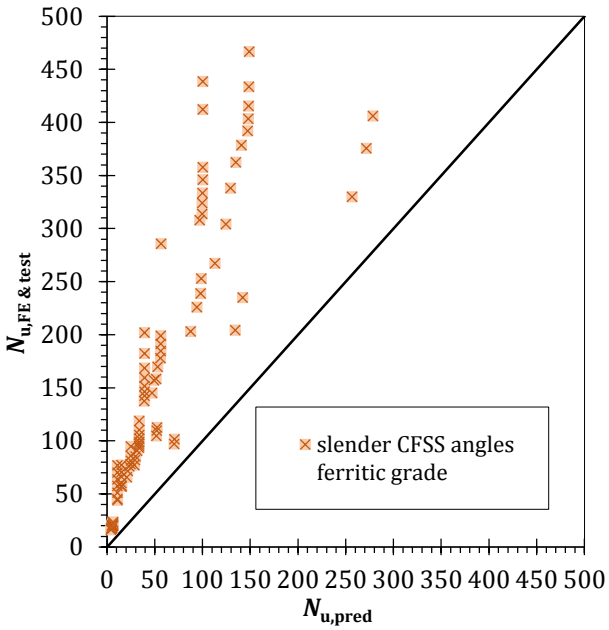

(e) EN 1993-1-4 / ferritic grade
$\alpha = 0.49$ $\bar{\lambda}_0 = 0.2$ & Eq. (7)

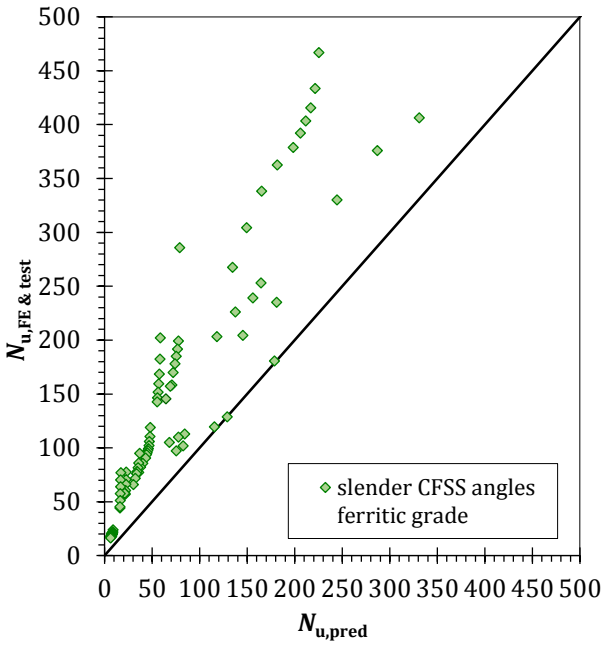

(f) AS/NZS 4673 / ferritic grade
Eqs. (15) & (17)

Fig. 13 Comparison of FE & test resistance with design resistance predictions for FTB.

Following the results of the comparative analysis, the following conclusions can be drawn:

- The results presented in Table 7 include two types of cross-section instability: (1) some of the angle sections undergo yielding and strain hardening before local buckling, and (2) the remaining ones undergo elastic local buckling before the yield stress is reached. It should be noted the Eurocode design procedure based on EWM does not always give the same prediction of cross-section class as FE modelling, in which the amplitude of initial local geometric imperfection of $+b/50$ was included; for certain data points, EN 1993-1-4 [20] predicts Class 3, whereas FE modelling predicts Class 4. In contrast to Eurocode, the AS/NZS [21] procedure provides more accurate predictions of the angle section ultimate strengths.

- It is evident from Fig. 9 that the non-dimensional limiting slenderness $\bar{\lambda}_0 = 0.4$ included in the current EN 1993-1-4 [20] design curve is unsuitable for CFSS equal-leg angle columns. In the very low slenderness range, the data trend exhibits a continuous decrease from full to reduced compressive capacities (caused by elastic local buckling and neutral axis shifting), with a transition point of approximately $\bar{\lambda}_0 = 0.2$ and 0.15 for ferritic and austenitic grade, respectively, whereas the data seems to suggest a higher plateau length for the duplex grade (approximately 0.30). These facts indicate that

the limiting non-dimensional slenderness smaller than 0.4 is more suitable for developing design buckling curves for CFSS equal-leg angle columns.

- Fig. 10 reveals a significant number of very unsafe minor-axis FB resistance predictions in the intermediate slenderness range, especially for the austenitic dataset ─ columns related to press-braked angles produced from hot-rolled austenitic strips. The study indicates that these columns have noticeably lower structural responses in comparison with their counterparts produced from cold-rolled austenitic strips. In addition to initial imperfections and effective centroid shifts, the dominant factor for strength degradation of angle columns produced from hot-rolled austenitic strips is the pronounced material non-linearity, i.e. the nonlinear softening of the material in the stress range between the proportionality limit and the yield strength.

- Comparisons of ultimate buckling resistances for the austenitic dataset, considering buckling curve *d* (α = 0.76, $\bar{\lambda}_0$ = 0.2), demonstrate that the European design method may be either conservative (for slender sections) or even excessively unconservative (particularly for non-slender sections), see Fig. 12a. The unsafe predictions are more significant for columns made from hot-rolled strips. For columns with non-slender angle sections failing in minor-axis FB, this curve results in FE & test-to-predicted ratios with a mean value of 1.181 and a CoV of 27.1%, as shown in Table 8. In contrast to austenitic grade, it can be seen from Fig. 12c and Fig. 12e that the predictive curve *c* (α = 0.49, $\bar{\lambda}_0$ = 0.2) is in good agreement with FE & test data for duplex and ferritic grades considering non-slender angle sections. The mean values of minor-axis FB resistance ratios are 1.007 and 1.159, with CoVs of 2.6% and 21.1% for duplex and ferritic grades, respectively (see Table 8).

- The interaction design procedure for columns with slender angle sections (axial compression & uniaxial minor-axis moment) gives acceptable and safe results but with considerable scatter in the data for all stainless steel grades. The mean ratios of FE & test-to-EN1993-1-4 predicted strengths, as reported in Table 8, are equal to 1.910, 2.054 and 1.953 with CoVs of 40.6%, 39.2% and 38.4% for austenitic, duplex and ferritic grades, respectively.

- The Australian codified procedure for CFSS angle columns provides more accurate and reliable resistance predictions (see Fig. 12b, Fig. 12d and Fig. 12f) with an noticeable lower scatter compared with Eurocode predictions. Similar to the EN 1993-1-4 design method, the AS/NSZ approach predicts the columns buckling by inelastic FB or by an interaction of the elastic cross-section buckling and minor-axis FB (the data points to slender angle-sections). Considering non-slender angle sections, the mean ratios of FE & test-to-AS/NSZ design predictions, as reported in Table 8, are equal to 1.157, 0.967 and 1.134 with CoVs of 22.9%, 2.9% and 19.4% for austenitic, duplex and ferritic grades, respectively. If local–global instability interactions occur, the mean values of resistance ratios are 1.630, 1.569 and 1.597, with CoVs of 30.3%, 26.3% and 26.8% for austenitic, duplex and ferritic grades, respectively.
- The FTB response of CFSS equal-leg angles is strongly associated with cross-section geometry. By increasing the leg widths, the distance between the shear centre and the section centroid, where the point of load application is located, increases, giving the tendency of the angle to twist in the entire overall slenderness range, independent of the column length. Considering the increase of the leg slenderness, the twisting of the angle section is then consequently accompanied by its elastic local buckling. In the currently presented parametric study, all generated FE data with FTB failure are related to slender angle sections (Class 4). It is evident from Fig. 11 that the FE & test data points with similar non-dimensional slenderness $\bar{\lambda}_{\mathrm{FT}}$, corresponding to angle section columns with the same cross-section size but different member lengths, show a high degree of scatter, with a significant number of unconservative data points for the austenitic grade. A similar data trend for both EN 1993-1-4 and AS/NSZ approaches can be found for FTB resistances, see Fig. 13. The mean ratios of FE & test-to-AS/NSZ design predictions, as presented in Table 8, are equal to 2.100, 2.470 and 2.360, with COVs of 29.7%, 24.7% and 26.9% for austenitic, duplex and ferritic grades, respectively, revealing that the Australian codified procedure yields less conservative and scattered FTB resistance predictions than Eurocode (see Table 8).

8. Flexural buckling curve proposal

The comparative design analysis presented in Section 7 revealed the significantly unsafe predictions for FE columns made from hot-rolled austenitic strip with cross-section geometry designated as ACF 70 × 70 × 8, ACF 70 × 70 × 10 and ACF 80 × 80 × 10, when the most conservative Eurocode buckling curve *d* (α = 0.76 $\bar{\lambda}_0$ = 0.2) is used to predict column compressive capacities. Fig. 14 demonstrates that the governing failure mode of these columns is inelastic minor-axis FB ─ the maximum axial compressive stresses at the leg tips (255–257 MPa) that are higher than the material yield strength f_y = 251 MPa (see Table 5) indicate that global instability occurs after the beginning of yielding. It is also worth noting that there is consistency between numerically obtained failure modes and the ones predicted by the EN 1993-1-4 design procedure (see Table 7) ─ the non-slender behaviour of the mentioned angle sections was validated by results of FE study.

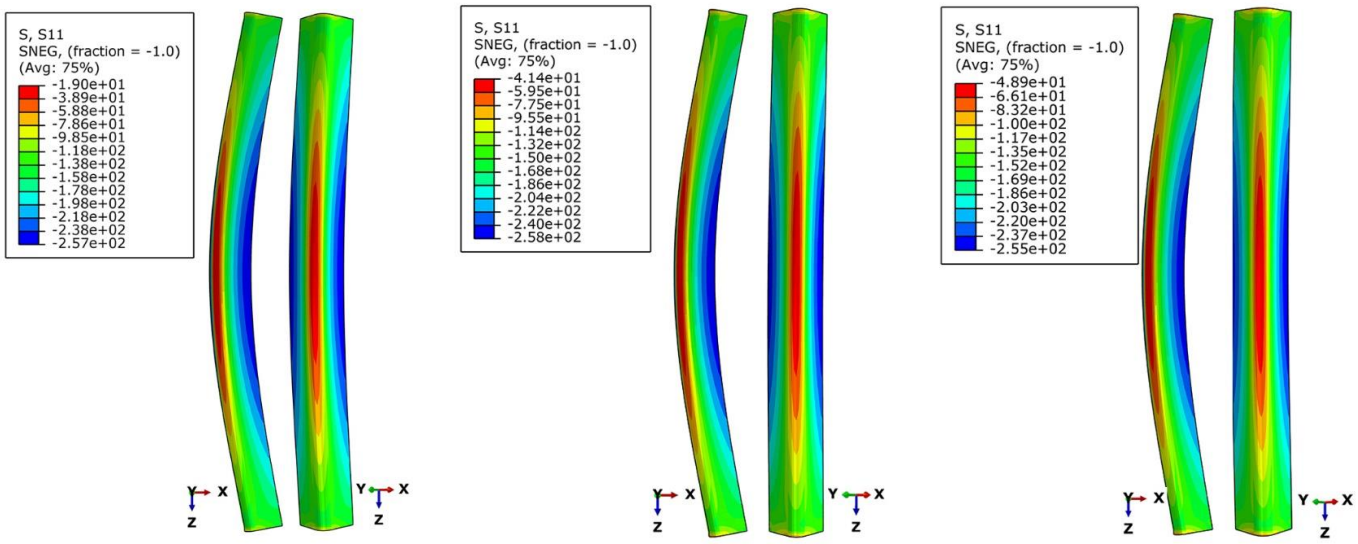

ACF 70 × 70 × 8, *L* = 900 mm ACF 70 × 70 × 10, *L* = 900 mm ACF 80 × 80 × 10, *L* = 1000 mm

Fig. 14 Minor-axis FB of columns produced from hot-rolled austenitic strip.

This section is focused on strength assessment of CFSS angle columns manufactured from hot-rolled (HR) and cold-rolled (CR) austenitic strips, with the aim to propose a new flexural buckling curve suitable for their design. A safe and efficient buckling curve that account for austenitic material non-linear law and achieves the target partial safety factor of γ_{M1} = 1.1 in EN 1993-1-4 [20] was sought. The proposed buckling curve is based on the Perry-Robertson formulation and developed by limiting non-dimensional slenderness to $\bar{\lambda}_0$ = 0.15 and the imperfection factor to α = 0.92. The proposed flexural buckling curve is plotted in Fig. 15 alongside the existing FE austenitic dataset. Its suitability and accuracy are graphically emphasized in Fig.

16, where the resistance ratios both for non-slender and slender sections are plotted against the minor-axis FB slenderness. The proposed curve is evaluated by means of reliability analysis in Section 9.

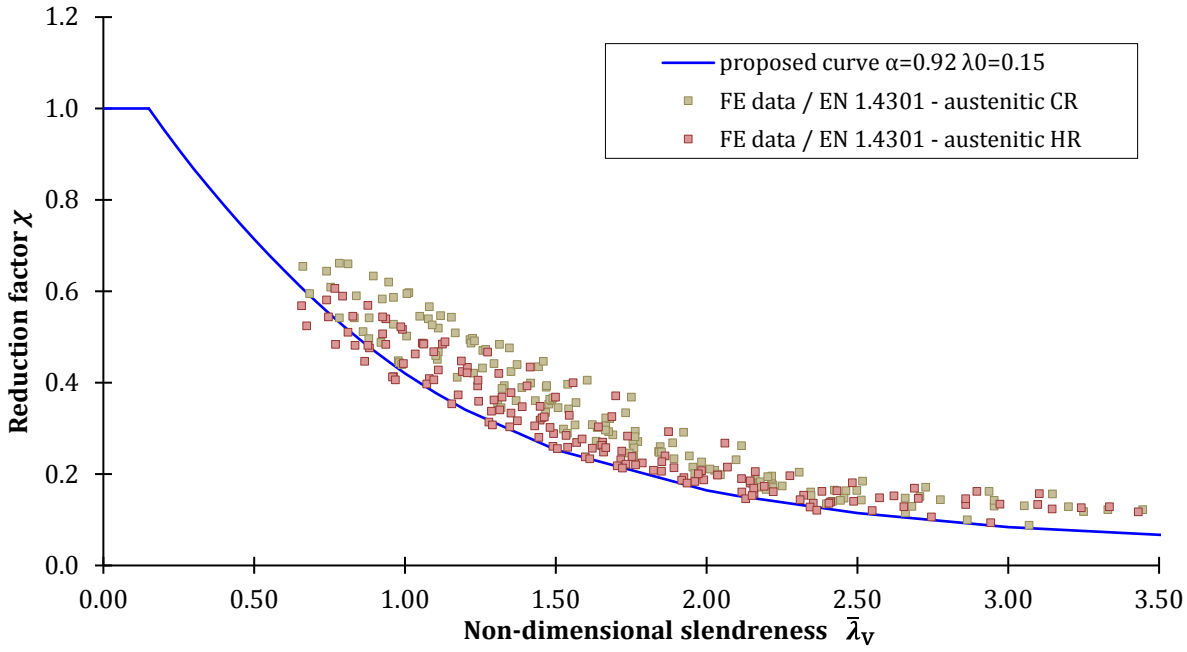

Fig. 15 Comparison between normalised FE & test results and proposed FB curve for austenitic grade.

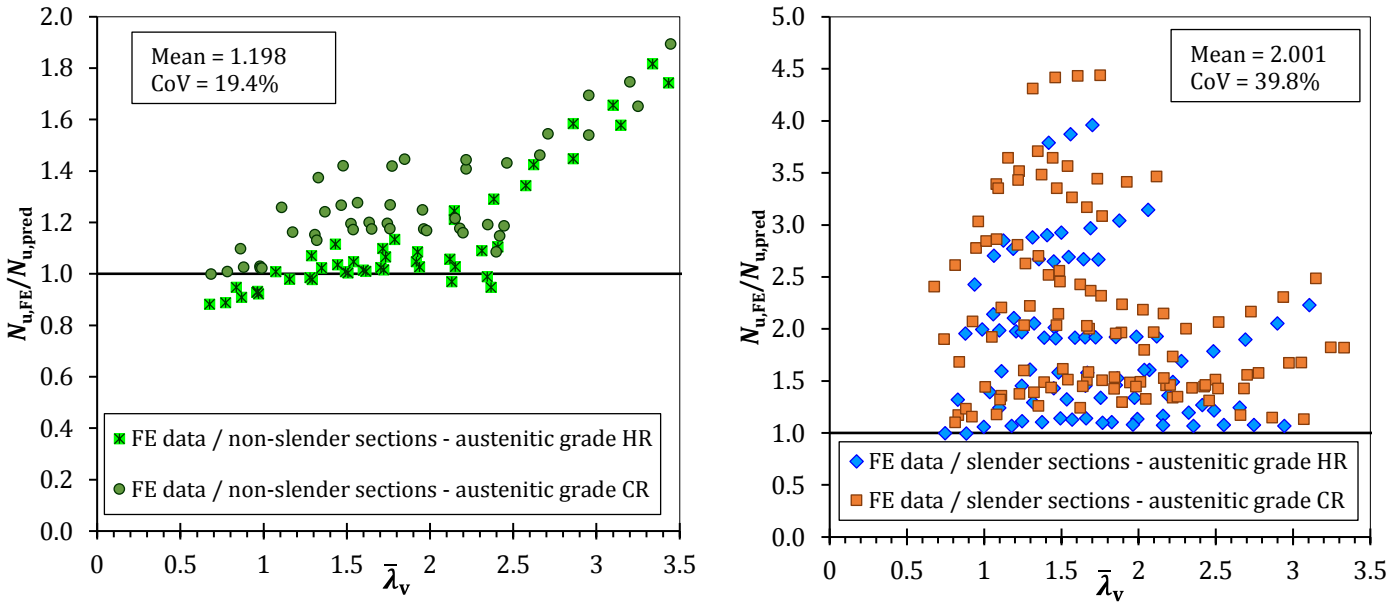

(a) Comparisons between FE data and design data for non-slender angle sections

(b) Comparisons between FE data and design data for slender angle sections

Fig. 16 Assessment of the proposed FB curve for austenitic grade stainless steel.

It can be seen from Fig. 16 that the proposed buckling curve offers improved fit to available data, providing a higher average ratio of the FE resistance-to-design resistance and less scatter across the austenitic datasets both for slender and non-slender angle sections, compared with the Eurocode buckling curve *d* (see Table 8).

Finally, the comparisons of minor-axis FB predictions between the AS/NZS design approach and the Eurocode procedure that includes the proposed buckling curve ($\bar{\lambda}_0$ = 0.15, α = 0.92) for austenitic grade, and buckling curve *c* for duplex and ferritic grades shown in Fig. 17, reveal a good correlation between the mentioned codes. However, the lower scatter in the data for the AS/NZS design approach is evident.

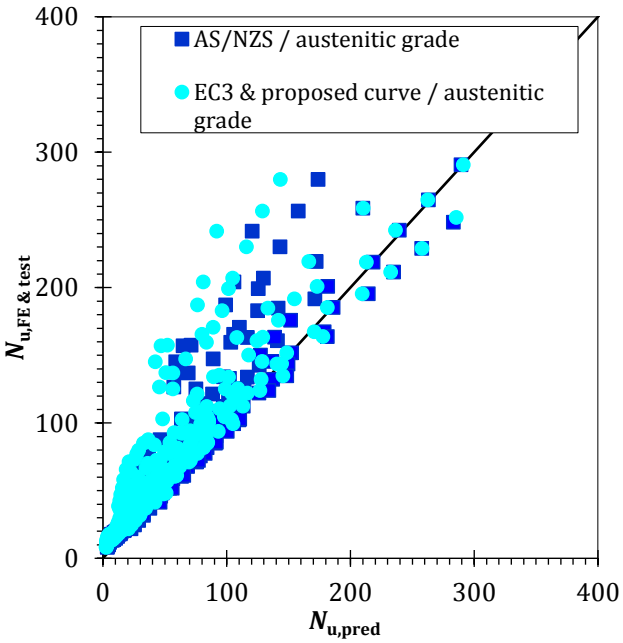

(a) Austenitic grade

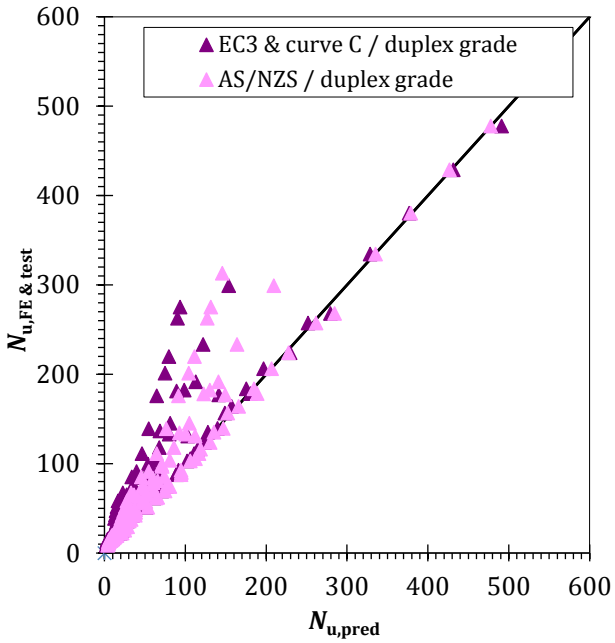

(b) Duplex grade

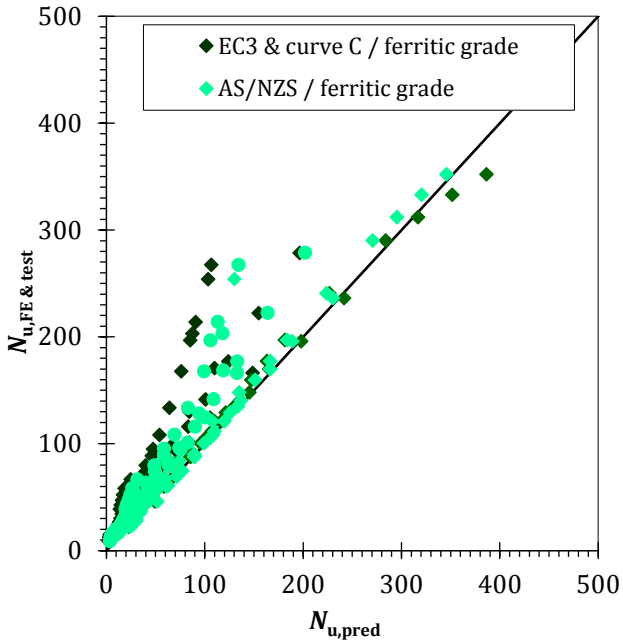

(c) Ferritic grade

Fig. 17 Comparisons of minor-axis FB predictions considering AS/NZS design procedure and Eurocode design procedure that include proposed curves.

9. Reliability assessment

9.1. Safety factor γ_{M1}

Statistical analyses in accordance with the procedure outlined in Annex D of EN 1990 [39] and the methodology described by Afshan et al. [40] were performed to assess the reliability of the proposed buckling curves for the CFSS equal-leg angle columns and calculate the values of the partial factors for member resistance γ_{M1} [20]. The FE results from the parametric studies performed in Section 6 and the collected test data [7], [8] are used in the statistical analyses. Following the provisions stated in Clause D8.2.2.5, Annex D of EN 1990 [39], the total population of the test was divided into sub-sets, depending on the group of data being considered, i.e., minor-axis FB, FTB or their interaction with uniaxial minor-axis moment, cross-section slenderness (non-slender and slender sections) and stainless steel grades. The described methodology allows using the total number of data points in the original series to assess the fractile factor avoiding large safety factors due to a smaller number of data points in each sub-set. It is worth emphasizing that the number of data points in each sub-set ultimately remained high. The material over-strength factors (representative of mean-to-nominal yield strength ratios) and CoV of yield strength were taken as 1.3 and 6.0% for austenitic, 1.1 and 3.0% for duplex and 1.2 and 4.5% for ferritic stainless steels, respectively, as recommended by Afshan et al. [40]; for the variability of the geometric properties, a CoV value of 5.0% was used [40].

Table 9 summarise the key statistical parameters, calculated based on 985 FE & test data points for CFSS equal-leg angle columns. The definitions of the parameters are as follows: n is the number of FE&test data; $k_{d,n}$ is the design (ultimate limit state) fractile factor; b is the average ratio of FE & test-to-model resistance based on a least squares fit to all the data; V_δ is the coefficient of variation of the FE & test data relative to the resistance model, and γ_{M1} is the partial safety factor for the buckling resistance.

Table 9. Results of the reliability assessment.

Grade	Cross-section Class	Dataset	$n\ (\bar{\lambda} > \bar{\lambda}_0)$	b	V_δ	γ_{M1}
EN 1993-1-4 / minor-axis FB (& minor-axis bending)						
Austenitic	Non-slender – Class 3	$\alpha = 0.76$ $\bar{\lambda}_0 = 0.2$	98	0.930	0.048	1.21
	Slender – Class 4	$\alpha = 0.76$ $\bar{\lambda}_0 = 0.2$ & Eq. (7)	193	1.455	0.231	1.21
	Non-slender – Class 3	proposed curve $\alpha = 0.92$ $\bar{\lambda}_0 = 0.15$	98	1.019	0.045	1.10
	Slender – Class 4	proposed curve $\alpha = 0.92$ $\bar{\lambda}_0 = 0.15$ & Eq. (7)	193	1.570	0.222	1.08
Duplex	Non-slender – Class 3	$\alpha = 0.49$ $\bar{\lambda}_0 = 0.2$	21	1.000	0.008	1.09
	Slender – Class 4	$\alpha = 0.49$ $\bar{\lambda}_0 = 0.2$ & Eq. (7)	119	1.948	0.226	1.03
Ferritic	Non-slender – Class 3	$\alpha = 0.49$ $\bar{\lambda}_0 = 0.2$	49	0.997	0.017	1.09
	Slender – Class 4	$\alpha = 0.49$ $\bar{\lambda}_0 = 0.2$ & Eq. (7)	85	1.624	0.194	1.09
EN 1993-1-4 / FTB & minor-axis bending						
Austenitic	Slender– Class 4	$\alpha = 0.34$ $\bar{\lambda}_0 = 0.2$ & Eq. (7)	212	1.880	0.270	1.09
Duplex	Slender– Class 4	$\alpha = 0.34$ $\bar{\lambda}_0 = 0.2$ & Eq. (7)	104	2.845	0.217	0.67
Ferritic	Slender– Class 4	$\alpha = 0.34$ $\bar{\lambda}_0 = 0.2$ & Eq. (7)	104	2.337	0.240	0.83

Based on the results of the reliability analysis, the following comments can be drawn:

- The assessment of European codified procedures confirms that the buckling curve *c* ($\alpha = 0.49$, $\bar{\lambda}_0 = 0.20$) provides reliable predictions for cold-formed equal-leg angle columns made from duplex and ferritic grades that fail due to minor-axis FB, considering both non-slender and slender angle sections. It should be noted that this does not comply to the proposal of the Design Manual for Structural Stainless Steel [23], where the more conservative buckling curve *d* ($\alpha = 0.76$, $\bar{\lambda}_0 = 0.20$) is adopted.
- For austenitic grade, buckling curve *d* provides unsatisfactory results for minor-axis FB, particularly for non-slender sections. The proposed new buckling curve ($\alpha = 0.92$, $\bar{\lambda}_0 = 0.15$) offers a resistance factor γ_{M1} that is equal to or lower than the current EN 1993-1-4 [20] value of 1.1, thus improving the accuracy and reliability of the strength evaluation.
- The reliability analyses show that the current design method covering the interaction of FTB and uniaxial minor-axis moment, stated in EN 1993-1-4 [20], gives significantly conservative but safe predictions with the resistance factors γ_{M1} lower than 1.1.

9.2. Resistance factor ϕ_c

To evaluate the AS/NZS 4673 [21] design method for CFSS equal-leg columns more quantitatively, the resistance factors ϕ_c were determined in accordance with the procedure described in Section K2.1.1 of AISI-

S100-16 [27] on the basis of the average values of the database. The LRFD (Load and Resistance Factor Design) resistance factor is defined as follows:

$$\phi_c = C_\phi (M_\mathrm{m} F_\mathrm{m} P_\mathrm{m}) e^{-\beta_0 \sqrt{V_M{}^2 + V_F{}^2 + C_P V_P{}^2 + V_Q{}^2}} \quad (18)$$

where C_ϕ = 1.52 is the calibration factor; M_m = 1.1 and F_m = 1.0 are the mean values of the Material (M) and Fabrication (F) factors; V_M = 0.1 and V_F = 0.05 are the coefficients of variation of the aforementioned factors (listed in Table K2.1.1-1 [27] for compressed members); β_o is the target reliability index for LRFD, which amounts to 2.5 for structural members; P_m and V_P are the mean value and the coefficient of variation of the Professional factor (P), expressed as the test-to-predicted strength ratio; V_Q is the coefficient of variation of load effect, which is equal to 0.21 for LRFD, and $C_\mathrm{P} = (1+1/n)m/(m-2)$ is the correction factor, where $m = n - 1$ represents the degrees of freedom and n represents the number of tests.

Mean FE & test-to-predicted ratios and the associated coefficient of variation for the AS/NZS design procedure are summarized in Table 10. The resistance factors listed in Table 10 are calculated using Eq. (18) for angle columns exposed to axial compression P and uniaxial minor-axis moment $P\cdot(L/1000 + e_\mathrm{N})$, where e_N is the shifting of the neutral axis of slender cross-sections. The reliability analyses show that the current design method in AS/NZS 4673 [21] for CFSS equal-leg angle columns provide precise, accurate and safe predictions with the resistance factor ϕ_c equal to or greater than the currently adopted codified value of 0.9. The results demonstrate there is potential for improvement of the current AS/NZS specification methods for CFSS equal-leg angle columns made from duplex grade.

Table 10. Results of the reliability assessment for AS/NZS 4673:2001.

Dataset	P_m	V_P	n	ϕ_c
Minor-axis FB				
All data	1.477	0.312	565	0.92
Austenitic	1.490	0.326	291	0.90
Duplex	1.496	0.290	140	0.97
Ferritic	1.426	0.300	134	0.91
FTB				
All data	2.310	0.278	420	1.54
Austenitic	2.101	0.297	212	1.35
Duplex	2.470	0.247	104	1.74
Ferritic	2.360	0.269	104	1.60

10. Conclusions

In the present paper, a comprehensive FE investigation of the structural responses of pin-ended cold-formed stainless steel equal-leg angle columns under compression was carried out. Minor-axis flexural buckling as well as flexural-torsional buckling were carefully addressed. The numerical parametric study included 996 FE models, previously validated by experiments from literature. Both slender and non-slender sections were examined over a wide range of column slenderness values including austenitic, duplex and ferritic alloys. The generated data, together with experimental data [6], [7], [8] were then compared with the current European EN 1993-1-4 [20] and Australian design methods AS/NZS 4673 [21]. The appropriateness of the different codified buckling curves (considering the shift of the centroid for Class 4 cross-sections) was evaluated per stainless steel family. Reliability analyses were undertaken according to the methodologies proposed in Annex D, EN 1990:2002 [39] and in Clause K2.1.1, AISI-S100-16 [27].

Based on the obtained results we conclude the following:

- The parameters α and $\bar{\lambda}_0$ which are respectively equal to 0.49 and 0.40 in the existing EN1993-1-4 [20] should be revised for the design of pin-ended cold-formed stainless steel equal-leg angle columns.
- For minor-axis flexural buckling, the buckling curve *c* (α = 0.49) in conjunction with the non-dimensional limiting slenderness $\bar{\lambda}_0$ = 0.2 may be used for ferritic and duplex grades for all cross-section classes. The safety factors γ_{M1} are lower than 1.10 for all cross-section classes.
- Following analysis of the assembled austenitic dataset, a new buckling curve for cold-formed austenitic equal-leg angle columns, of the same form as the existing European curves, was proposed, with the higher imperfection factor α = 0.92 and with a reduced limiting slenderness $\bar{\lambda}_0$ = 0.15, with the aim of offering safe, but efficient predictions. The safety factors γ_{M1} are equal to 1.10 and 1.09 for non-slender and slender and angle sections, respectively.
- The use of buckling curve *b* (α = 0.49) in conjunction with $\bar{\lambda}_0$ = 0.2 to predict flexural-torsional buckling leads to safe but quite conservative results characterized by significantly higher scatter and safety factors lower than 1.10 for all three stainless steel grades.

- Comparing the results to the current AS/NZS [21] specification predictions indicate that the design procedure that treats angle columns subjected to concentric compression as beam-columns under eccentric compression safely and accurately quantifies column compressive capacities, especially for minor-axis flexural buckling failure. Similar to Eurocode 3, the design procedure addresses flexural-torsional buckling results with significantly conservative predictions of the column ultimate strengths. It was confirmed that the LRFD resistance factor $\phi_c = 0.9$, currently prescribed in AS/NZS [21] for the design of compression members, can be adopted for the failure load prediction of pin-ended cold-formed stainless steel equal-leg angle columns.

Funding

This investigation is supported by the Serbian Ministry of Education, Science and Technological Development through the TR-36048 project.

Declarations of interest: none

Acknowledgements

The authors are grateful to companies Montanstahl ag Switzerland, Vetroelektrane Balkana Belgrade, Armont SP Belgrade, Institute for Testing of Materials Belgrade, Institute for Materials and Structures Faculty of Civil Engineering University of Belgrade, ConPro Novi Sad, Energoprojekt Industrija PLC Belgrade, Vekom Geo Belgrade, CO-Designing, Peri Oplate Belgrade, North Engineering Subotica, Amiga Kraljevo, Mašinoprojekt kopring PLC Belgrade, Sika Belgrade, DvaD Solutions Belgrade and Soko Inžinjering Belgrade for their support.

References

[1] N.R. Baddoo, Stainless steel in construction: A review of research, applications, challenges and opportunities, J. Constr. Steel Res. 64 (11) (2008) 1199–1206.

[2] B. Rossi, Discussion on the use of stainless steel in constructions in view of sustainability, Thin-Walled Struct. 83 (2014) 182-189.

[3] J. Dobrić, B. Rossi, Column curves for stainless steel lipped channel sections, J. Struct. Eng., ASCE, 146 (10) (2020) 1-14.

[4] J. Dobrić, D. Buđevac, Z. Marković, N. Gluhović, Behaviour of stainless steel press-braked channel sections under compression, J. Construct. Steel Res. 139 (2017) 236–253.

[5] J. Dobrić, J. Ivanović, B. Rossi, Behaviour of stainless steel plain channel section columns, Thin-Walled Struct., 148 (2020) 2-16.

[6] H. Kuwamura, Local Buckling of Thin-Walled Stainless Steel Members, Steel Structures, 3 (2003) 191-201.

[7] L. Zhang, K. Hai Tan, O Zhao, Experimental and numerical studies of fixed-ended cold-formed stainless steel equal-leg angle section columns, Thin-Walled Struct., 184 (2019)134–144.

[8] J. Dobrić, A. Filipović, Z. Marković, N. Baddoo, Structural response to experimental axial testing of cold-formed stainless steel equal angle columns, Thin-Walled Struct., 156 (2020) 1-16.

[9] A. Filipović, J. Dobrić, Z. Marković, N. Baddoo, M. Spremić, N. Fric, Experimental investigation of compressed stainless steel angle columns, SDSS 2019 - International Colloquium on Stability and Ductility of Steel Structures.

[10] K.J.R. Rasmussen, Design of angle columns with locally unstable legs, J. Struct. Eng., ASCE 131(10) (2005) 1553–60.

[11] N. Silvestre, P.B. Dinis, D. Camotim, Developments on the design of cold-formed steel angles, J. Struct. Eng., ASCE 139 (5) (2013) 680–94.

[12] P.B. Dinis, D. Camotim, A novel DSM-based approach for the rational design of fixed-ended and pin-ended short-to-intermediate thin-walled angle columns, Thin-Walled Struct. 87(February) (2015)158–82.

[13] A. Landesmann, D. Camotim, P.B. Dinis, R. Cruz, Short-to-intermediate slender pinended cold-formed steel equal-leg angle columns: experimental investigation, numerical simulations and DSM design, Eng. Struct., 132 (2017) 471–93.

[14] T.B. Peköz, Development of a Unified Approach to the Design of Cold-Formed Steel Members, Report SG-86-4, American Iron and Steel Institute, 1986.

[15] D. Popovic, G.J. Hancock, K.J.R. Rasmussen, Axial compression tests of cold-formed angles, J Struct Eng, ASCE 125(5) (1999) 515–523.

[16] D. Popovic, G.J. Hancock, K.J.R. Rasmussen, Compression tests on cold-formed angles loaded parallel with a leg, J. Struct. Eng., ASCE, 2001;127(6):600–607.

[17] B. Young, Tests and design of fixed-ended cold-formed steel plain angle columns. J. Struct. Eng., ASCE 130(12) (2004)1931–40.

[18] E. Ellobody, B. Young, Behavior of cold-formed steel plain angle columns, J. Struct. Eng., ASCE 131(3) (2005) 457–66.

[19] G.M.B. Chodraui, Y. Shifferaw, M. Malite, B.W. Schafer, Cold-formed steel angles under axial compression, LaBoube R, Yu WW, editors, Proceedings of 18th international specialty conference on cold-formed steel structures (Orlando, 26–27/10) 285–300.

[20] Eurocode 3: Design of steel structures – part 1-4: General rules – supplementary rules for stainless steels, including amendment A1 (2015), EN 1993-1-4:2006+A1:2015, Brussels, Belgium, CEN 2015.

[21] AS/NZS 4673:2001: Cold-formed stainless steel structures. Australian – New Zealand Standard. Standards Australia, 2001.

[22] Eurocode 3: Design of steel structures – Part 1-5: Plated structural elements EN 1993-1-5, Brussels, Belgium, CEN 2006.

[23] S. Afshan, I. Arrayago, N. Baddoo, L. Gardner, G. Gedge, M. Jandera, E. Real, B. Rossi, N. Stranghöner, O. Zhao, Design manual for structural stainless steel, Berkshire: The Steel Construction Institute, 2017.

[24] Eurocode 3: Design of Steel Structures – Part 1-3: General rules - Supplementary rules for cold-formed members and sheeting EN 1993-1-3, Brussels, Belgium, CEN 2006.

[25] Eurocode 3: Design of steel structures – Part 1-1: General rules and rules for buildings EN 1993-1-1, Brussels, Belgium, CEN 2005.

[26] SEI/ASCE 8-02: Specification for the Design of Cold-Formed Stainless Steel Structural Members, American Society of Civil Engineers, 2003.

[27] AISI-S100-16 (2016), North American Specification for the Design of Cold-Formed Steel Structural Members, AISI Standard, American iron and Steel Institute.

[28] K.J.R. Rasmussen, J. Rondal, Column curves for stainless steel alloys. J. Construct. Steel. Res., 54 (2000) 89–107.

[29] K. J. R. Rasmussen, J. Rondal, Explicit Approach to Design of Stainless Steel Columns, J. Struct. Eng., ASCE 123(7) (1997) 857-863.

[30] ABAQUS User Manual. Version 6.12. Providence, RI, USA: DS SIMULIA Corp; 2012.

[31] Y. Huang, B. Young, Experimental investigation of cold-formed lean duplex stainless steel beam-columns, Thin-Walled Struct., 76 (2014) 105–117.

[32] B. Rossi, S. Afshan, L. Gardner, Strength enhancements in cold-formed structural sections – Part II: Predictive models, J. Constr. Steel Res., 83 (2013) 189–196.

[33] K.J.R. Rasmussen, G.J. Hancock, Design of cold-formed stainless steel tubular members I: Columns, J. Struct. Eng., ASCE 119 (8) (1993) 2349–2367.

[34] L. Gardner, D. A. Nethercot, Numerical modeling of stainless steel structural components a consistent approach, J. Struct. Eng., ASCE 130 (10) (2004) 1586–1601.

[35] EN 1090-2: Execution of steel structures and aluminium structures – Part 2: Technical requirements for steel structures. Brussels, Belgium, CEN 2008.

[36] M. Lecce, K. J. Rasmussen, Distortional Buckling of Cold-Formed Stainless Steel Sections: Experimental Investigation, J Struct Eng., ASCE 132 (4) (2006) 497–504.

[37] B. Rossi, J.-P. Jaspart, K. J. Rasmussen, Combined distortional and overall flexural-torsional buckling of cold-formed stainless steel sections: Experimental investigations, Journal of Structural Engineering. 136 (4) (2010) 354–360.

[38] I. Arrayago, E. Real, L. Gardner, Description of stress-strain curves for stainless steel alloys, Materials and Design, 87 (2015) 540-552.

[39] Eurocode: Basis of structural design EN 1990, Brussels, Belgium, European Committee for Standardization (CEN); 2002.

[40] S. Afshan, P. Francis, N. R. Baddoo, L. Gardner, Reliability analysis of structural stainless steel design provisions, J. Construct. Steel Res., 114 (2015) 293–304.